TABLE 4. Genes Showing Higher Expression in Advanced-Stage Tumors

No.	Accession number	Symbol	Description	S/N value
1	M87339	*RFC4*	Human replication factor C	−2.112
2	L76191	*IRAK1*	Interleukin-1 receptor-associated kinase 1	−1.801
3	U66619	*SMARCD3*	SWI/SNF related, subfamily d, member 3	−1.733
4	M91670	*UBE2S*	Ubiquitin-conjugating enzyme E2S	−1.677
5	D64142	*H1FX*	Histone family, member X	−1.652
6	U37689	*POLR2H*	Polymerase (RNA) II polypeptide H	−1.519
7	M27830	*RNR1*	Human 28S ribosomal RNA gene	−1.442
8	Z97074	*RAB9P40*	Rab9 effector p40	−1.433
9	HG960-HT960	*SOS*	Son of sevenless homolog 1 (Drosophila)	−1.348
10	L24559	*POLA2*	Polymerase (DNA-directed), alpha (70kD)	−1.309
11	U65402	*GPR31*	Seven transmembrane G-couples receptor	−1.295
12	X73066	*NME1*	Non-metastatic cells 1, NM23-H1	−1.287
13	L19686	*MIF*	Macrophage migration inhibitor factor	−1.277
14	HG3729-HT3999	*HSHPX5*	Homeotic protein Hpx-5	−1.207
15	D78586	*CAD*	Carbamoyl-phosphate synthetase 2	−1.205
16	D14678	*KIFC1*	Kinesin family member C1	−1.171
17	HG4074-HT4344	*FEN1*	Flap structure-specific endonuclease 1	−1.167
18	U90426	*DDX5*	Nuclear RNA helicase	−1.166
19	D14889	*DDX39*	DEAD (Asp-Glu-Ala-Asp) box polypeptide 39	−1.161
20	U73379	*UBE2C*	Ubiquitin-conjugating enzyme E2C	−1.159
21	X74795	*MCM5*	Minichromosome maintenance deficient 5	−1.157
22	U64871	*LTB4R*	Gprotein-coupled receptor	−1.152
23	U14394	*TIMP3*	Tissue inhibitor of metalloproteinase 3	−1.101
24	U76638	*BARD1*	BRCA1 associated RING domain 1	−1.091
25	D55716	*MCM7*	Minichromosome maintenance deficient 7	−1.063
26	HG919-HT919	*POLEDNA*	Polymerase (DNA directed), epsilon	−1.054
27	S69370	*PAX3B*	Transcription factor	−1.051
28	L25876	*CDKN3*	Cyclin-dependent kinase inhibitor 3	−1.017
29	M13228	*MYCN*	Human N-myc oncogene	−1.007
30	U07664	*HB9*	Human HB9 homeobox gene	−1.001

S/N value reflects the difference between early and advanced stages of the patients. The genes examined by real-time PCR are indicated by underlining.

by two-way clustering analysis. Supplementary data are available at http://www2.genome.rcast.u-tokyo.ac.jp/NBL/supp.html.

Relationship between Clinicopathological Findings and Expression of *API2*, *p19INK4D*, and *BAF60c* Genes in NB

Because the functions of the *BIRC3*, *CDKN2D*, and *SMARCD3* genes are known to be related to apoptosis, the cell cycle, and transcriptional activation, respectively (Guan et al., 1996; Wang et al., 1996; LaCasse et al., 1998), it is possible that these genes are involved in the progression of NB. Thus, to clarify the biological significance of the expression of these genes in NB, we did additional quantitative real-time PCR analysis on a total of 50 NB samples. The *TRKA* and *NME1* genes were excluded from this study because they are already known as prognostic factors in NB (Leone et al., 1993; Nakagawara et al., 1993; Godfriend et al., 2002). Normal adrenal gland tissue (Clontech) was used as the control, and target gene expression was normalized to that of *β-actin*. The expression of the *BIRC3* gene was significantly higher in stage-1 and -2 patients than in stage-4 patients ($P = 0.002$ and 0.001; Fig. 5A). Furthermore, significantly higher expression of the *BIRC3* gene was observed in the tumors detected by our mass screening program than in those detected by the clinical course ($P = 0.031$). *BIRC3* expression was also significantly higher in the patients under 1 year of age than in those more than 1 year old ($P = 0.021$). Much higher expression of the *BIRC3* gene was detected in only 1 of 4 tumors with *MYCN* amplification, and the average expression level of the *BIRC3* gene in the tumor with *MYCN* amplification was low. *BIRC3* expression in the normal adrenal gland was as low as in the tumors of stage-4 and -4S patients (Fig. 5A).

The expression of the *CDKN2D* gene was significantly higher in stage-1 and -2 patients than in stage-4 patients ($P = 0.012$ and 0.009; Fig. 5C). Expression of *CDKN2D* just as significantly high was observed in both groups detected by the mass screening program and in infants ($P = 0.04$). Ex-

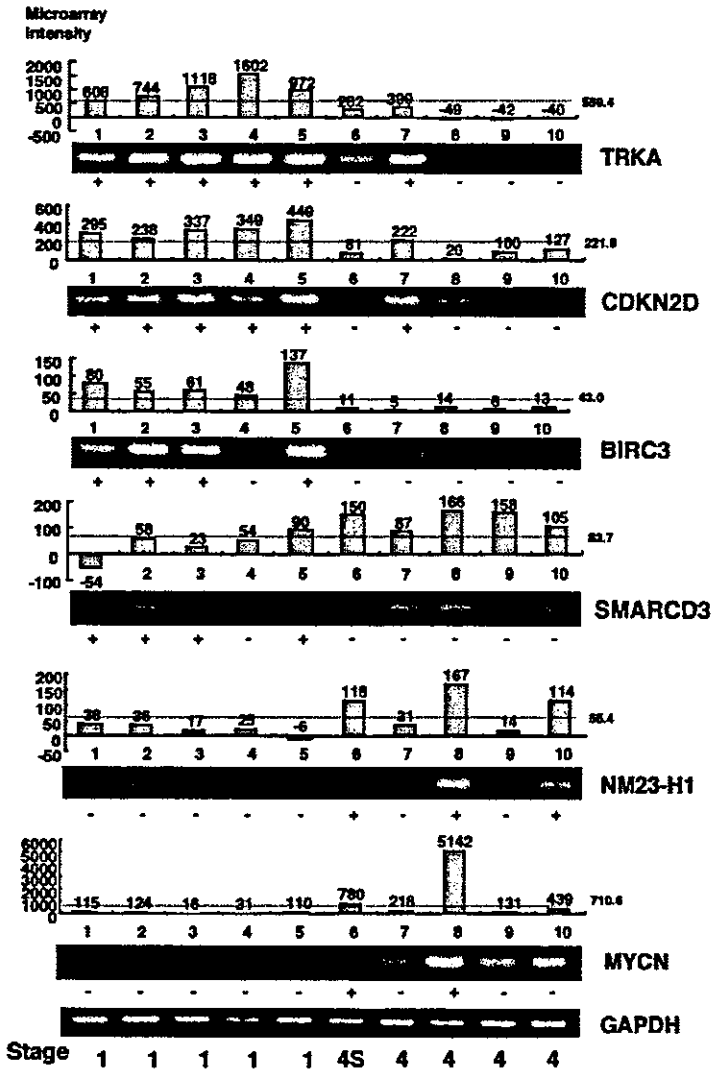

Figure 3. Semiquantitative RT-PCR analysis. Representative results for 10 of the 20 samples examined are shown in this figure. The upper three genes are those that showed higher expression in early-stage tumors, and the lower three genes those that showed higher expression in advanced-stage tumors. GAPDH was used as a control. The microarray intensity score of each gene also is indicated. The mean microarray intensity score of each gene is indicated as a dotted line.

tremely low *CDKN2D* expression was found in tumors with *MYCN* amplification. The *CDKN2D* expression in the normal adrenal gland was higher than in the tumors of stage-4 and -4S patients (Fig. 5C).

SMARCD3 expression was significantly higher in stage-4 patients than in stage-1 and -2 patients ($P = 0.03$ and 0.038, respectively). Although the tumor of the stage-4S patient had a tendency to higher *SMARCD3* expression than that of stage-1 and -2 patients, no significant difference was observed. High expression of the *SMARCD3* gene was detected in all patients with *MYCN* amplification. *SMARCD3* expression in the normal adrenal gland was as low as in the tumors of stage-1, -2, and -3 patients (Fig. 5 D). To investigate the correlation between the expression of the genes as measured by microarray and by real-time PCR analyses, we compared the intensity score of *BIRC3* determined by microarray and real-time PCR analyses in 20 samples (Fig. 6). As shown in Figure 6, the coefficient was as high as 0.968 ($n = 20$, $P < 0.0001$), indicating that the expression intensity of *BIRC3* detected by microarray analysis corresponded well to that detected by real-time PCR analysis.

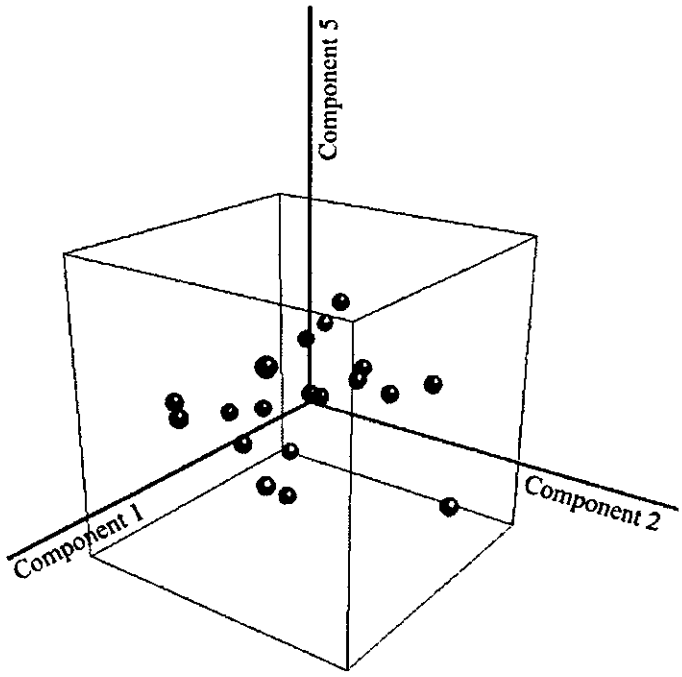

Figure 4. PCA three-dimensional plot of the 20 samples. Stage-of-disease subgroups (stages 1, 2, 4S, and 4) are indicated. Blue plots represent tumors classified as stage 1, green plots those classified as stage 2, red plots those classified as stage 4, and pink plots those classified as stage 4S.

Expression of *BIRC3*, *CDKN2D*, and *SMARCD3* Genes in NB Cell Lines

We also analyzed the expression patterns of the *BIRC3*, *CDKN2D*, and *SMARCD3* genes in 27 NB cell lines with real-time PCR analysis. The expression of these three genes was detected in all 27 cell lines. Significantly lower expression of both the *BIRC3* and *CDKN2D* genes was observed in the cell lines than in the primary tumors of NB (P = 0.002 and 0.003, respectively), whereas expression of the *SMARCD3* gene was significantly higher in the cell lines than in the primary NB tumors (P = 0.001).

Expression of *BIRC2*, *SMARCD1*, and *SMARCD2* Genes in NB

The *BIRC3* gene has a high homology to the *BIRC2* gene, and these two genes sit in tandem on chromosome band 11q21, with an intergenic distance of approximately 7 kb (Young et al., 1999). The tissue distributions and functions of the *BIRC2* and *BIRC3* genes appear to be similar, although the relative expression of the *BIRC3* is generally higher (Young et al., 1999). Moreover, the *SMARCD3* gene has two homologs, *SMARCD1* and *SMARCD2*, and they share 70%–80% identity with each other (Wang et al., 1996). Thus, to determine whether the *BIRC2*, *SMARCD1*, and *SMARCD2* genes could be additional prognostic markers for NB, we further examined these gene expression patterns in 50 primary tumors and 27 cell lines of NB by real-time RT-PCR analysis. Generally, low expression levels of the *BIRC2* gene were detected in the adrenal gland, primary tumors, and cell lines of NB, indicating obvious differences in expression patterns between *BIRC2* and *BIRC3* in NB (Fig. 5A and B). Despite the extremely high expressions of *SMARCD1* and *SMARCD2* in the cell lines, both genes showed low expression in the primary tumors. No significantly different expression patterns of these genes between the early and advanced stages of NB were observed (Fig. 5E and F).

DISCUSSION

We have shown the global gene expression profiles of NB and that we were able to identify genes that are differentially expressed between the early and advanced stages of NB. The results of RT-PCR analysis of the several identified genes were concordant with the microarray analysis data, confirming the fidelity of the system. By two-way clustering analysis, the 20 NB samples were classified into two main phylogenic groups, indicating the existence of at least two major genetic subgroups in

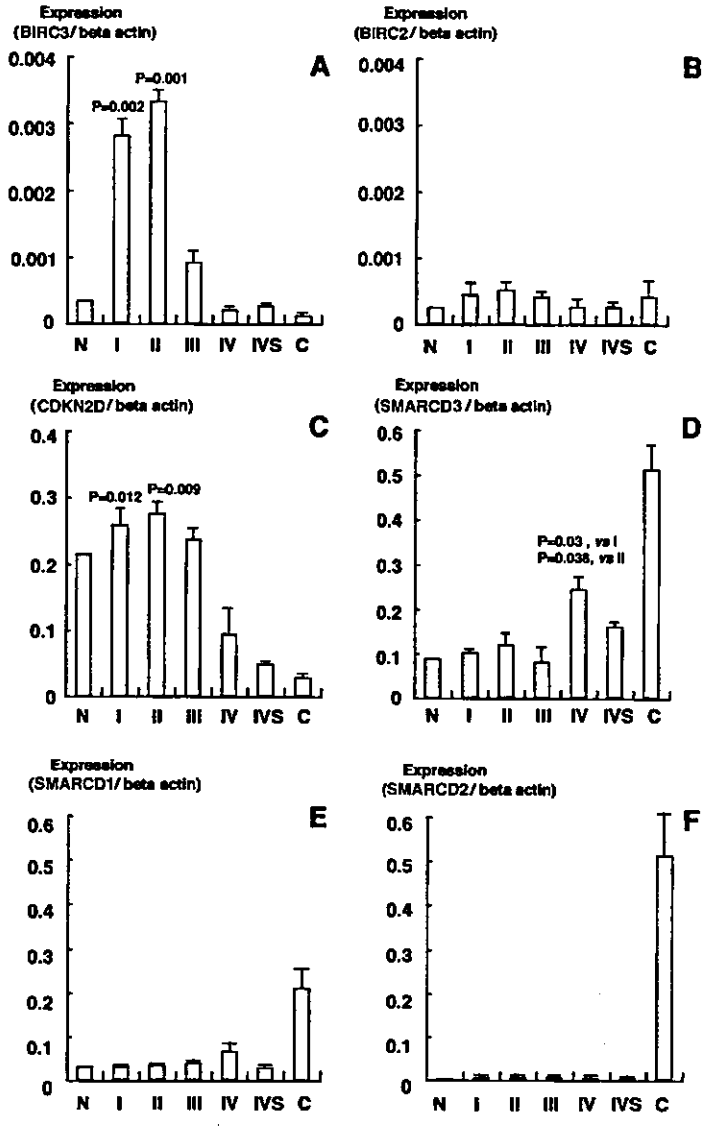

Figure 5. Real-time PCR analysis in neuroblastoma. The mean expression levels of each stage of patients and cell lines were standardized by the β-actin level. The expression of *BIRC3* and *CDKN2D* was significantly higher in stage-1 and -2 tumors than in those of stage 4. *SMARCD3* expression was also significantly higher in stage-4 tumors than in those of stages 1 and 2 according to Welch's test (N, normal adrenal; C, cell lines).

the tumors examined. Most early- and advanced-stage tumors were classified into similar expression profiling subgroups, group 1 and group 2, respectively. However, the remaining tumors in each group revealed obviously different expression patterns. Therefore, these variations in gene expression patterns suggest heterogeneity in the tumors in both the early and the advanced stages of NB. *MYCN* amplification is known to be the best-characterized genetic alteration associated with the prognosis for NB outcome. In this study, one tumor with *MYCN* amplification showed an expression pattern distinct from that of 3 other tumors with *MYCN* amplification, suggesting that *MYCN*-independent pathways exist in the progression of NB.

To gain a better insight into the structure of the microarray data, we used PCA and plotted the data in three-dimensional scaling. In this analysis, histologic subgroups and stages of the disease were found to be clearer classification methods than two-way clustering analysis. Thus, two-way clustering analysis only separated the data by histologic and clinical variation in expression patterns. Because we used only a limited number of tumors, addi-

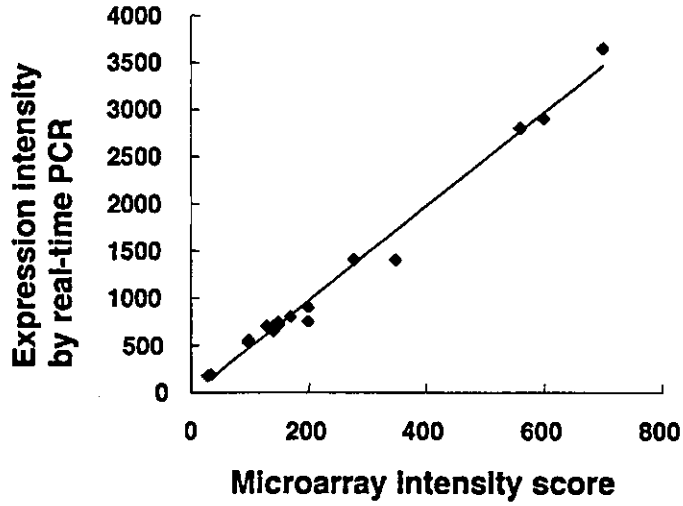

Figure 6. Scatter graph of intensity scores of *BIRC3* by microarray and real-time PCR analyses in 20 samples. Microarray intensity score and expression intensity score by real-time PCR are plotted on a logarithmic scale on the abscissa and ordinate, respectively. The coefficient was as high as 0.968 ($n = 20$, $P < 0.0001$).

tional studies that use a larger number of NB samples are required to provide conclusive data for the microarray analysis and PCA.

As the *BIRC3*, *CDKN2D*, and *SMARCD3* genes have been reported to be associated with apoptosis, the cell cycle, and transcriptional activation, respectively, it is possible that these genes are involved in the progression of NB. Thus, among the genes differentially expressed, we further investigated the *BIRC3*, *CDKN2D*, and *SMARCD3* genes by real-time PCR analysis. The *BIRC3* gene belongs to the inhibitors of apoptosis (IAP) family and has been reported to inhibit the apoptosis pathway by blocking caspase activity (LaCasse et al., 1998; Young et al., 1999). Recently, Survivin, a member of the IAP family, has been demonstrated to inhibit the apoptosis of NB cells (Islam et al., 2000). Moreover, *NAIP*, another member of the IAP family, has been reported to suppress neuronal differentiation and apoptosis in PC12 cells (Gotz et al., 2000). In the present study, *BIRC3* expression was up-regulated in the early-stage tumors, whereas Survivin has been reported to be highly expressed in the advanced stage of NB. These facts suggest that *BIRC3* could play an important role in suppressing neuronal apoptosis in the favorable group of NB, just as Survivin does in unfavorable groups. Moreover, the *BIRC3* gene is on chromosome band 11q21 and has been reported to be fused to the *MALT1* gene in mucosa-associated lymphoid tissue (MALT) lymphoma with t(11;18)(q21;q21) (Dierlamm et al., 1999; Motegi et al., 2000). Generally, MALT lymphoma is characterized by an indolent clinical behavior and a good prognosis (Dierlamm et al., 1999). The *BIRC3–MALT1* fusion products have been thought to lead to inhibition of germinal-center B-cell apoptosis and the subsequent development of MALT lymphomas (Motegi et al., 2000). Thus, this outcome and our results both suggest that *BIRC3* is involved in the genesis and/or progression of several human cancers, especially tumors with a good prognosis. The *BIRC3* gene has high homology with the *BIRC2* gene, and these two genes are located in tandem on 11q21 (Young et al., 1999). The functions and tissue distributions of these two genes appeared similar (Young et al., 1999). However, we found obviously different expression patterns between *BIRC2* and *BIRC3* in NB, indicating that the *BIRC3*, but not the *BIRC2*, gene would be functional in NB.

The *CDKN2D* gene, a cyclin-dependent kinase (CDK) inhibitor, was more highly expressed in the early-stage tumors. This gene is a member of the inhibitors of CDK4 (INK4) family and directly blocks not only CDK4, but also CDK6 (Guan et al., 1999). There is accumulating evidence that genetic alterations of the *CDKN2A* and *CDKN2B* genes, both members of the INK4 family, are involved in the biologic behavior of many different types of human cancers, such as melanoma, lung carcinoma, and acute lymphoblastic leukemia (Ranade et al., 1995; Xiao et al., 1995; Maloney et al., 1999). Furthermore, we previously reported that the *CDKN2A* gene might be a candidate tumor-suppressor gene involved in the progression of NB (Takita et al., 1997, 1998). However, unlike the alterations in the *CDKN2A* and *CDKN2B* genes, alterations of the *CDKN2D* gene are rare in human cancers (Zariwala

et al., 1996), and *CDKN2D*-deficient mice showed no development of tumors (Zindy et al., 2000). Therefore, it is possible that *CDKN2D* is not a potent tumor-suppressor gene in human cancers. However, recently, it has been demonstrated that mice lacking both *CDKN2D* and *CDKN1B* showed ectopic neuronal cell divisions and apoptosis in many parts of the brain that were normally quiescent (Zindy et al., 1999). The *CDKN2D* and *CDKN1B* proteins, therefore, cooperate to prevent cell division within the brain and maintain differentiated neurons in a quiescent state (Zindy et al., 1999). Thus, a high expression of *CDKN2D* in early-stage NB may suggest that this protein plays a role in preventing the cell proliferation of a favorable type of NB cells.

We found that *SMARCD3*, a member of the SWI/SNF complex family, was expressed significantly more in the advanced stage of NB. The SWI/SNF complex is known to be a chromatin-remodeling enzyme, and it has been implicated in the transcriptional activation of a number of genes through chromatin remodeling (Wang et al., 1996). Recently, the *SNF5/INI1* gene, on chromosome band 22q21, a member of the SWI/SNF complex family, was identified as a tumor-suppressor gene for malignant rhabdoid tumor in children (Versteege et al., 1998; Uno et al., 2002). Furthermore, mice lacking the *Snf5/Ini1* gene have been reported to stop developing at the peri-implantation stage, and heterozygous mice develop vertebral tumors showing features of neural-crest-derived cells (Guidi et al., 2001). These findings and the present results suggest that the *SMARCD3* gene might be involved in the genesis and/or progression of NB. Although the *SMARCD3* gene has two homologs, *SMARCD1* and *SMARCD2*, the expression patterns of these two genes were different from *SMARCD3*, indicating the presence of a specific role of *SMARCD3* in NB.

In conclusion, we showed that there are genetic subsets in NB and that some of the genes of interest are differentially expressed, including *BIRC3*, *CDKN2D*, and *SMARCD3*, which have never been reported to be associated with NB. Thus, microarray technology is a good system for identifying such genes. From the microarray technology results together with the results of real-time PCR analysis in additional NB samples, it has been shown that it is likely that, in addition to the *MYCN*, *TRKA*, and *RASH* genes, the *BIRC3*, *CDKN2D*, and *SMARCD3* genes also have an important prognostic value in NB. Only a limited number of cases were analyzed in our study, and a large-scale study would allow a detailed classification of NB.

ACKNOWLEDGMENTS

We thank Mrs. S. Sohma and Mrs. H. Soga for their excellent technical assistance. We also express our appreciation to Dr. K. Nishimura, Advanced Science and Technology, University of Tokyo, for his kind direction of the PCA analysis, and to Dr. A. T. Look, Harvard Medical School, and Dr. A. Inoue, St. Jude Children's Research Hospital, for their generous gift of NB cell lines.

REFERENCES

Brodeur GM, Seeger RC, Schwab M, Varmus HE, Bishop JM. 1984. Amplification of N-myc in untreated human neuroblastomas correlates with advanced disease stage. Science 224:1121–1124.

Brodeur GM, Maris JM, Yamashiro DJ, Hogarty MD, White PS. 1997. Biology and genetics of human neuroblastomas. J Pediatr Hematol Oncol 19:93–101.

Chen YY, Takita J, Chen YZ, Yang HW, Hanada R, Yamamoto K, Hayashi Y. 2003. Genomic structure and mutational analysis of the human KIF1Bα gene located at 1p36.2 in neuroblastoma. Int J Oncol 23:737–744.

Chen YZ, Soeda E, Yang HW, Takita J, Chai L, Horii A, Inazawa J, Ohki M, Hayashi Y. 2001. Homozygous deletion in neuroblastoma cell line defined by a high-density STS map spanning human chromosome band 1p36. Genes Chromosomes Cancer 31:326–332.

Dierlamm J, Baens M, Wlodarska I, Stefanova-Ouzounova M, Hernandez JM, Hossfeld DK, De Wolf-Peeters C, Hagemeijer A, Van den Berghe H Marynen P. 1999. The apoptosis inhibitor gene API2 and a novel 18q gene, MLT, are recurrently rearranged in the t(11;18)(q21;q21) associated with mucosa-associated lymphoid tissue lymphomas. Blood 93:3601–3609.

Gershon D. 2002. Microarray technology: an array of opportunities. Nature 416:885–891.

Godfried MB, Veenstra M, Sluis P, Boon K, Asperen R, Hermus MC, Schaik BD, Voute TP, Schwab M, Versteeg R Caron HN. 2002. The N-myc and c-myc downstream pathways include the chromosome 17q genes nm23-H1 and nm23-H2. Oncogene 21: 2097–2101.

Gotz R, Karch C, Digby MR, Troppmair J, Rapp UR, Sendtner M. 2000. The neuronal apoptosis inhibitory protein suppresses neuronal differentiation and apoptosis in PC12 cells. Hum Mol Genet 9:2479–2489.

Guan KL, Jenkins CW, Li Y, O'Keefe CL, Noh S, Wu X, Zariwala M, Matera AG, Xiong Y. 1996. Isolation and characterization of $p19^{INK4d}$, a p16-related inhibitor specific to CDK6 and CDK4. Mol Biol Cell 7:57–70.

Guidi CJ, Sands AT, Zambrowicz BP, Turner TK, Demers DA, Webster W, Smith TW, Imbalzano AN, Jones SN. 2001. Disruption of INI1 leads to peri-implantation lethality and tumorigenesis in mice. Mol Cell Biol 21:3598–3603.

Inoue A, Yokomori K, Tanabe H, Mizusawa H, Sofuni T, Hayashi Y, Tsuchida Y, Shimatake H. 1997. Extensive genetic heterogeneity in the neuroblastoma cell line NB (TU)1. Int J Cancer 72:1070–1077.

Ishii M, Hashimoto S, Tsutsumi S, Wada Y, Matsushima K, Kodama T, Aburatani, H. 2000. Direct comparison of GeneChip and SAGE on the quantitative accuracy in transcript profiling analysis. Genomics 68:136–143.

Islam A, Kageyama H, Takada N, Kawamoto T, Takayasu H, Isogai E, Ohira M, Hashizume K, Kobayashi H, Kaneko Y, Nakagawara A. 2000. High expression of Survivin, mapped to 17q25, is significantly associated with poor prognostic factors and promotes cell survival in human neuroblastoma. Oncogene 19:617–623.

Kaneko M, Tsuchida Y, Uchino J, Takeda T, Iwafuchi M, Ohnuma N, Mugishima H, Yokoyama J, Nishihira H, Nakada K, Sasaki S, Sawada T, Kawa K, Nagahara N, Suita S, Sawaguchi S. 1999. Treatment results of advanced neuroblastoma with the first Japanese study group protocol. Study Group of Japan for Treatment of Advanced Neuroblastoma. J Pediatr Hematol Oncol 2:190–197.

Kitanaka C, Kato K, Ijiri R, Sakurada K, Tomiyama A, Noguchi K, Nagashima Y, Nakagawara A, Momoi T, Toyoda Y, Kigasawa H, Nishi T, Shirouzu M, Yokoyama S, Tanaka Y, Kuchino Y. 2002. Increased Ras expression and caspase-independent neuroblastoma cell death: possible mechanism of spontaneous neuroblastoma regression. J Natl Cancer Inst 94:358–368.

Knudson AG. 2001. Two genetic hits (more or less) to cancer. Nat Rev Cancer, 2:157–162.

Kong XT, Choi SH, Inoue A, Xu F, Chen T, Takita J, Yokota J, Bessho F, Yanagisawa M, Hanada R, Yamamoto K, Hayashi Y. 1997. Expression and mutational analysis of the DCC, DPC4, and MADR2/JV18–1 genes in neuroblastoma. Cancer Res 57:3772–3778.

LaCasse EC, Baird S, Korneluk RG, MacKenzie AE. 1998. The inhibitors of apoptosis (IAPs) and their emerging role in cancer. Oncogene 17:3247-3259.

Leone A, Seeger RC, Hong CM, Hu YY, Arboleda MJ, Brodeur GM, Stram D, Slamon DJ, Steeg PS. 1993. Evidence for nm23 RNA overexpression, DNA amplification and mutation in aggressive childhood neuroblastomas. Oncogene 8:855–865.

Maloney KW, McGavran L, Odom LF, Hunger SP. 1999. Acquisition of p16 (INK4A) and p15 (INK4B) gene abnormalities between initial diagnosis and relapse in children with acute lymphoblastic leukemia. Blood 93:2380–2385.

Motegi M, Yonezumi M, Suzuki H, Suzuki R, Hosokawa Y, Hosaka S, Kodera Y, Morishima Y, Nakamura S, Seto M. 2000. API2-MALT1 chimeric transcripts involved in mucosa-associated lymphoid tissue type lymphoma predict heterogeneous products. Am J Pathol 156:807–812.

Mukasa A, Ueki K, Matsumoto S, Tsutsumi S, Nishikawa R, Fujimaki T, Asai A, Kirino T, Aburatani H. 2002. Distinction in gene expression profiles of oligodendrogliomas with and without allelic loss of 1p. Oncogene 21:3961–3968.

Nakagawara A, Arima-Nakagawara M, Scavarda NJ, Azar CG, Cantor AB, Brodeur GM. 1993. Association between high levels of expression of the TRK gene and favorable outcome in human neuroblastoma. N Engl J Med 328:847–854.

Nakao M, Janssen JW, Flohr T, Bartram CR. 2000. Rapid and reliable quantification of minimal residual disease in acute lymphoblastic leukemia using rearranged immunoglobulin and T-cell receptor loci by LightCycler technology. Cancer Res 60:3281–3289.

Ohira M, Kageyama H, Mihara M, Furuta S, Machida T, Shishikura T, Takayasu H, Islam A, Nakamura Y, Takahashi M, Tomioka N, Sakiyama S, Kaneko Y, Toyoda A, Hattori M, Sakaki Y, Ohki M, Horii A, Soeda E, Inazawa J, Seki N, Kuma H, Nozawa I, Nakagawara A. 2000. Identification and characterization of a 500-kb homozygously deleted region at 1p36.2–p36.3 in a neuroblastoma cell line. Oncogene 19:4302–4307.

Ranade K, Hussussian CJ, Sikorski RS, Varmus HE, Goldstein AM, Tucker MA, Serrano M, Hannon GJ, Beach D, Dracopoli NC. 1995. Mutations associated with familial melanoma impair $p16^{INK4}$ function. Nat Genet 10:1114–1116.

Schwab M. 1997. MYCN Amplification in neuroblastoma: a paradigm for the clinical use of an oncogene. Pathol Oncol Res 3:3–7.

Smith EI, Haase GM, Seeger RC, Brodeur GM. 1989. A surgical perspective on the current staging in neuroblastoma—the International Neuroblastoma Staging System proposal. J Pediatr Surg 24:386–390.

Takita J, Hayashi Y, Kohno T, Shiseki M, Yamaguchi N, Hanada R, Yamamoto K , Yokota J. 1995. Allelotype of neuroblastoma. Oncogene 11:1829-1834.

Takita J, Hayashi Y, Kohno T, Yamaguchi N, Hanada R, Yamamoto K, Yokota J. 1997. Deletion map of chromosome 9 and p16 (CDKN2A) gene alterations in neuroblastoma. Cancer Res 57: 907–912.

Takita J, Hayashi Y, Nakajima T, Adachi J, Tanaka T, Yamaguchi N, Ogawa Y, Hanada R, Yamamoto K , Yokota J. 1998. The p16 (CDKN2A) gene is involved in the growth of neuroblastoma cells and its expression is associated with prognosis of neuroblastoma patients. Oncogene 17:3137–3147.

Takita J, Hayashi Y, Takei K, Yamaguchi N, Hanada R, Yamamoto K, Yokota J. 2000. Allelic imbalance on chromosome 18 in neuroblastoma. Eur J Cancer 36:508–513.

Takita J, Yang HW, Chen YY, Hanada R, Yamamoto K, Teitz T, Kidd V, Hayashi Y. 2001. Allelic imbalance on chromosome 2q and alterations of the caspase 8 gene in neuroblastoma. Oncogene 20:4424–4432.

Tanaka T, Sugimoto T, Sawada T. 1998. Prognostic discrimination among neuroblastomas according to Ha-ras/trk A gene expression: a comparison of the profiles of neuroblastomas detected clinically and those detected through mass screening. Cancer 83:1626–1633.

Teitz T, Wei T, Valentine MB, Vanin EF, Grenet J, Valentine VA, Behm FG, Look AT, Lahti JM, Kidd VJ. 2000. Caspase 8 is deleted or silenced preferentially in childhood neuroblastomas with amplification of MYCN. Nat Med 6:529–535.

Uno K, Takita J, Yokomori K, Tanaka Y, Ohta S, Shimada H, Gilles FH, Sugita K, Abe S, Sako M, Hashizume K, Hayashi Y. 2002. Aberrations of the hSNF5/INI1 gene are restricted to malignant rhabdoid tumors or atypical teratoid/rhabdoid tumors in pediatric solid tumors. Genes Chromosomes Cancer 34:33–41.

Versteege I, Sevenet N, Lange J, Rousseau-Merck MF, Ambros P, Handgretinger R, Aurias A, Delattre O. 1998. Truncating mutations of hSNF5/INI1 in aggressive paediatric cancer. Nature (Lond) 94:203–206.

Wai DH, Schaefer KL, Schramm A, Korsching E, Van Valen F, Ozaki T, Boecker W, Schweigerer L, Dockhorn-Dworniczak B, Poremba C. 2002. Expression analysis of pediatric solid tumor cell lines using oligonucleotide microarrays. Int J Oncol 20:441–451.

Wang W, Xue Y, Zhou S, Kuo A, Cairns BR, Crabtree GR. 1996. Diversity and specialization of mammalian SWI/SNF complexes. Genes Dev 10:2117–2130.

Xiao S, Li D, Corson JM, Vijg J, Fletcher JA. 1995. Codeletion of p15 and p16 genes in primary non-small cell lung carcinoma. Cancer Res 55:2968–2971.

Yamamoto K, Hanada R, Kikuchi A, Ichikawa M, Aihara T, Oguma E, Moritani T, Shimanuki Y, Tanimura M, Hayashi Y. 1998. Spontaneous regression of localized neuroblastoma detected by mass screening. J Clin Oncol 16:1265–1269.

Yang HW, Piao HY, Chen YZ, Takita J, Kobayashi M, Taniwaki M, Hashizume K, Hanada R, Yamamoto K, Taki T, Bessho F, Yanagisawa M, Hayashi Y. 2000. The p73 gene is less involved in the development but involved in the progression of neuroblastoma. Int J Mol Med 5:379–384.

Yang HW, Chen YZ, Takita J, Soeda E, Piao HY, Hayashi Y. 2001a. Genomic structure and mutational analysis of the human KIF1B gene which is homozygously deleted in neuroblastoma at chromosome 1p36.2. Oncogene 20:5075–5083.

Yang HW, Chen YZ, Piao HY, Takita J, Soeda E, Hayashi Y. 2001b. DNA fragmentation factor 45 (DFF45) gene at 1p36.2 is homozygously deleted and encodes variant transcripts in neuroblastoma cell line. Neoplasia 3:165–169.

Yeoh EJ, Ross ME, Shurtleff SA, Williams WK, Patel D, Mahfouz R, Behm FG, Raimondi SC, Relling MV, Patel A, Cheng C, Campana D, Wilkins D, Zhou X, Li J, Liu H, Pui CH, Evans WE, Naeve C, Wong L, Downing JR. 2002. Classification, subtype discovery, and prediction of outcome in pediatric acute lymphoblastic leukemia by gene expression profiling. Cancer Cell 1:133–143.

Young SS, Liston P, Xuan JY, McRoberts C, Lefebvre CA, Korneluk RG. 1999. Genomic organization and physical map of the human inhibitors of apoptosis: HIAP1 and HIAP2. Mamm Genome 10: 44–48.

Zariwala M, Xiong Y. 1996. Lack of mutation in the cyclin-dependent kinase inhibitor, $p19^{INK4d}$, in tumor-derived cell lines and primary tumors. Oncogene 13:2033—2038.

Zindy F, Cunningham JJ, Sherr CJ, Jogal S, Smeyne RJ, ussel MF. 1999. Postnatal neuronal proliferation in mice lacking Ink4d and Kip1 inhibitors of cyclin-dependent kinases. Proc Natl Acad Sci USA 96:13462–13467.

Zindy F, van Deursen J, Grosveld G, Sherr CJ, Roussel MF. 2000. INK4d-deficient mice are fertile despite testicular atrophy. Mol Cell Biol 20:372–378.

THE JOURNAL OF BIOLOGICAL CHEMISTRY
© 2004 by The American Society for Biochemistry and Molecular Biology, Inc.

Vol. 279, No. 25, Issue of June 18, pp. 26475–26480, 2004
Printed in U.S.A.

Nuclear Factor of Activated T-cells (NFAT) Rescues Osteoclastogenesis in Precursors Lacking c-Fos*

Received for publication, December 22, 2003, and in revised form, March 11, 2004
Published, JBC Papers in Press, April 8, 2004, DOI 10.1074/jbc.M313973200

Koichi Matsuo‡§¶‖, Deborah L. Galson,‡‡¶ Chen Zhao‡¶, Lan Peng**, Catherine Laplace**, Kent Z. Q. Wang§§, Marcus A. Bachler§, Hitoshi Amano¶¶, Hiroyuki Aburatani‖‖, Hiromichi Ishikawa‡, and Erwin F. Wagner§**

*From the ‡Department of Microbiology and Immunology, School of Medicine, Keio University, Tokyo 160-8582, Japan, §Research Institute of Molecular Pathology (IMP), A-1030 Vienna, Austria, **New England Baptist Bone and Joint Institute, Department of Medicine, Beth Israel Deaconess Medical Center and Harvard Medical School, Boston, Massachusetts 02115, ‡‡Center for Bone Biology, Department of Medicine, and §§Department of Molecular Genetics and Biochemistry, School of Medicine, University of Pittsburgh, Pittsburgh, Pennsylvania 15213, ¶¶Department of Pharmacology, School of Dentistry, Showa University, Tokyo 142-8555, Japan, and the ‖‖Research Center for Advanced Science and Technology, University of Tokyo, Tokyo 153-8904, Japan*

Osteoclasts are specialized macrophages that resorb bone. Mice lacking the AP-1 component c-Fos are osteopetrotic because of a lack of osteoclast differentiation and show an increased number of macrophages. The nature of the critical function of c-Fos in osteoclast differentiation is not known. Microarray analysis revealed that *Nfatc1*, another key regulator of osteoclastogenesis, was down-regulated in $Fos^{-/-}$ osteoclast precursors. Chromatin immunoprecipitation assay showed that c-Fos bound to the *Nfatc1* and *Acp5* promoters in osteoclasts. *In vitro* promoter analyses identified nuclear factor of activated T-cells (NFAT)/AP-1 sites in the osteoclast-specific *Acp5* and *Calcr* promoters. Moreover, in $Fos^{-/-}$ precursors gene transfer of an active form of NFAT restored transcription of osteoclast-specific genes in the presence of receptor activator of the NF-κB ligand (RANKL), rescuing bone resorption. In the absence of RANKL, however, $Fos^{-/-}$ precursors were insensitive to NFAT-induced osteoclastogenesis unlike wild-type precursors. These data indicate that lack of *Nfatc1* expression is the cause of the differentiation block in $Fos^{-/-}$ osteoclast precursors and that transcriptional induction of *Nfatc1* is a major function of c-Fos in osteoclast differentiation.

AP-1 refers to a family of dimeric transcription factors composed of Fos (c-Fos, Fra1, Fra2, and FosB) and Jun proteins (1, 2). Transcription factors such as nuclear factor-κB (NF-κB)[1] and AP-1, both critically involved in osteoclast differentiation, are activated in the presence of macrophage/colony-stimulating factor (M-CSF, also known as CSF-1) and receptor activator of NF-κB ligand (RANKL) (3, 4). These cytokines induce signals via multiple pathways including mitogen-activated protein kinases, phosphatidylinositol 3-kinase and calcium (3, 5, 6). The essential role for c-Fos during osteoclast differentiation (7–9) is partially explained by the observations that the expression of all Fos family proteins is down-regulated in $Fos^{-/-}$ precursors and that other Fos proteins such as Fra1 can rescue the differentiation of these precursors (10, 11). Therefore, a role of c-Fos appears to enhance production of Fos proteins during osteoclastogenesis. c-Fos also transcriptionally induces β-interferon, which then negatively regulates osteoclastogenesis by down-regulating c-Fos at the protein level (12). Beyond the Fos family, however, c-Fos target genes that rescue osteoclastogenesis in $Fos^{-/-}$ precursors are not known.

NFATc1 is a member of the NFAT (nuclear factor of activated T-cells) family of transcription factors (NFATc1, NFATc2, NFATc3, and NFATc4, as accepted by HUGO and the Genome Data Base, corresponding to NFAT2, NFAT1, NFAT4, and NFAT3, respectively) (13–15). It has been shown to be up-regulated following RANKL treatment and is important for osteoclast differentiation (5, 16, 17). In this study, we explore the cause of the differentiation block in $Fos^{-/-}$ precursors by analyzing transcriptional target genes of c-Fos, especially *Nfatc1*, during osteoclast differentiation.

EXPERIMENTAL PROCEDURES

Cell Culture—ST2-T cells were established by infecting the mouse stromal line ST2 with the retroviral vector expressing RANKL (18). For co-culture, bone marrow cells or splenocytes were seeded at 6×10^5 cells/cm^2 with 6×10^4/cm^2 ST2-T cells and cultured in the presence of 10^{-8} M 1,25-dihydroxyvitamin D_3 and 10^{-7} M dexamethasone. For osteoblast-free culture, non-adherent hematopoietic precursor cells were cultured in the presence of 10 ng/ml recombinant human M-CSF (Genzyme) and 10–30 ng/ml recombinant mouse RANKL (R&D Systems). RAW264.7 cells were obtained from ATCC (TIB-71). Transient transfection was performed using LipofectAMINE (Invitrogen).

Microarray—Oligonucleotide microarrays (GeneChip Murine Genome U74Av2, Affymetrix) were used to monitor the relative abundance of transcripts. Gene Expression Omnibus accession numbers: $Fos^{+/+}$ splenocytes (GSM10341), $Fos^{-/-}$ splenocytes (GSM10342), $Fos^{+/+}$ bone marrow (GSM10343), $Fos^{-/-}$ splenocytes expressing ΔNFAT (GSM10344), $Fos^{-/-}$ splenocytes expressing green fluorescent protein (GFP) (GSM10345).

Western Blotting—Total cell extracts were prepared in a standard SDS lysis buffer. Nuclear extracts were prepared as described (19).

* This work was supported by the Suzuken Memorial Foundation (to K. M.), National Institutes of Health Grant AR45421 (to D. L. G.), an Arthritis Foundation Fellowship Award (to C. L.), Grant-in-aid for Creative Scientific Research by the Japan Society for the Promotion of Science 13GS0015 (to H. I.), Boehringer Ingelheim (which supports the Research Institute of Molecular Pathology (IMP)) (to E. F. W.), and the Program for Promotion of Fundamental Studies in Health Science of the Organization for Pharmaceutical Safety and Research of Japan (number MF-14). The costs of publication of this article were defrayed in part by the payment of page charges. This article must therefore be hereby marked "*advertisement*" in accordance with 18 U.S.C. Section 1734 solely to indicate this fact.

¶ These authors contributed equally to this work.
‖ To whom correspondence should be addressed. Tel.: 81-3-3353-1211 (ext. 61223); Fax: 81-3-5360-1508; E-mail: matsuo@sc.itc.keio.ac.jp.

[1] The abbreviations used are: NF-κB, nuclear factor-κB; M-CSF, macrophage/colony-stimulating factor; RANKL, receptor activator of NF-κB ligand; NFAT, nuclear factor of activated T-cells; GFP, green fluorescent protein; EMSA, electrophoretic mobility shift assay; IL, interleukin; TRAP, tartrate-resistant acid phosphatase.

Immunofluorescence—Mature osteoclasts were prepared from femurs of 3-day-old wild-type mice by curetting with a scalpel into medium. After 1 h incubation, cells were fixed in 4% paraformaldehyde and permeabilized in 0.1% Triton X-100 and 1% bovine serum albumin in phosphate-buffered saline. Primary antibodies used were anti-NFATc1 (7A6) or anti-NFATc2 (G1-D10).

Plasmids—Mouse *Acp5*-luciferase reporter plasmid was constructed in pGL3 vector (Promega) by transferring the promoter regions (−1453 down to the end of intron 1) from pKB5 (a gift from D. Roodman), and the NFAT site mutation was introduced by using the QuikChange kit (Stratagene). ΔNFAT was constructed by assembling PCR-amplified fragments encoding amino acids 1–239 of enhanced GFP (Clontech) followed by Ser-Arg (an XbaI site) and amino acids 317–902 of human NFATc4 (20). The 2.5-kb ΔNFAT fragment was cloned into both the cytomegalovirus-driven expression vector pRK5 and the retroviral vector pMX (21). pBJ5-human NFATc1 expression plasmid (pSH102) was a gift from G. R. Crabtree. The −797 and −94 *Calcr*-P3-pGL3basic constructs have been described (22). Additional *Calcr*-P3 5′-deletion constructs were generated by PCR using different forward *Calcr* primers with a BglII site and a common reverse *Calcr* primer with a HindIII site. The NFAT site mutations were incorporated into each deletion by sequential PCR reactions using mutant *Calcr* primers and vector primers. The c-Fos expression vector pMX-c-Fos-IRES-GFP was constructed by inserting the BamHI-SalI fragment of mouse c-*Fos* cDNA in pBabe-c-Fos (10). The sequence of each construct was confirmed. The small interfering RNA vectors were based on RVH1 and LTRH1 (23) (a gift from R. Medzhitov). The oligonucleotides encoding the mouse c-Fos small interfering RNA were: RNAi1, 5′-gatcccctgatgttctcgggtttcaattcaagagattgaaacccgagaacatcatttttggaac-3′ and 5′-tcgagttccaaaaatgatgttctcgggtttcaatctcttgaattgaaacccgagaacatcaggg-3′; RNAi2, 5′-gatcccctccaagcggagacagatcattcaagagatgatctgtctccgcttggatttttggaac-3′ and 5′-tcgagttccaaaaatccaagcggagacagatcatctcttgaatgatctgtctccgcttggaggg-3′.

Electrophoretic Mobility Shift Assay (EMSA)—Oligonucleotide sequences for *Acp5* EMSA were: *Acp5*-120 (the NFAT/AP-1 site in the human *Acp5* promoter), 5′-cgagccctcggagaaactgcatcatcctcg-3′, 5′-tcgacgaggatgatgcagtttctccgagggctcgagct-3′; IL-2 (the distal NFAT/AP-1 site in the human IL-2 promoter), 5′-cgagaaggaggaaaaactgtttcatacagg-3′, 5′-tcgacctgtatgaaacagtttttcctccttctcgagct-3′; consensus AP-1 (the AP-1 site in the human collagenase promoter), 5′-cgagataaagcatgagtcagacacctcg-3′, 5′-tcgacgaggtgtctgactcatgctttatctcgagct-3′; mutated AP-1, 5′-cgagataaagcaagagtctgacacctcg-3′, 5′-tcgacgaggtgtcagactcttgctttatctcgagct-3′.

Oligonucleotide sequences for *Calcr* EMSA were: *Calcr*-2, 5′-ggaacatgacagctcatttccatgttccct-3′; *Calcr*-2mA, 5′-ggaacattcacgctcatttccatgttccct-3′; *Calcr*-2mN, 5′-ggaacatgacagctccgggccatgttccct-3′; AP-1, 5′-cgcttgatgactcagccggaa-3′. Recombinant NFATc1 protein was synthesized *in vitro* from wtNFATc1-pCITE4 plasmid (a gift from N. A. Clipstone). Competition reactions included a 200-fold molar excess of unlabeled oligonucleotides.

Real-time Reverse Transcriptase-PCR—*Calcr* transcripts were quantitated on ABI PRISM 7000 (Applied Biosystems) using SYBR Green and were normalized to c-*fms* and *Gapdh* transcripts for co-cultures and osteoblast-free cultures, respectively.

Bone Resorption Assay—The surface of bone slices was visualized by backscattered electron imaging using a scanning electron microscope (S-2500CX, Hitachi). The extent of bone resorption was quantified with Metamorph (Universal Imaging).

Chromatin Immunoprecipitation—The chromatin immunoprecipitation assay was performed as described previously (24). Polyclonal anti-c-Fos antibody (Ab-2, Oncogene) or normal rabbit IgG (sc-2027, Santa Cruz Biotechnology) were used. Immunoprecipitated DNA fragments were quantified by real-time PCR on ABI PRISM 7000. The PCR primers used were: *Nfatc1*-disF046, 5′-cgcccatgcaatctgttagtaa-3′; *Nfatc1*-disR248, 5′-gcctgagaaagctactctccc-3′; *Acp5*-1474F, 5′-tgcccagtacacattaccatcag-3′; *Acp5*-1715R, 5′-ggaccaaaagcggtgatcac-3′.

RESULTS

NFATc1 Is Down-regulated in $Fos^{-/-}$ Osteoclast Precursors—We set out to identify genome-wide novel c-Fos target genes in the osteoclast lineage. Three osteoclastogenic cultures derived from wild-type and $Fos^{-/-}$ splenocytes and wild-type bone marrow were prepared and co-cultured with stromal ST2-T cells. By day 6, the wild-type cultures produced abundant multinucleated osteoclasts, which were tartrate-resistant acid phosphatase (TRAP)-positive, whereas no such cells were generated in the $Fos^{-/-}$ culture (data not shown). The co-cultured cells were harvested *in toto*, and gene expression was analyzed by microarrays. The genes in which expression was detectable in wild-type cultures but absent or very low in the $Fos^{-/-}$ culture are summarized in Table I. The numbers for wild-type splenocytes (Sp+/+), $Fos^{-/-}$ splenocytes (Sp−/−), and wild-type bone marrow cells (Bm+/+) are GeneChip scores indicating RNA levels. In the $Fos^{-/-}$ culture, the expression of *Nfatc1* was undetectable, and the expression of known osteoclast marker genes (25) was reduced. These include *Acp5* (encoding TRAP), *Ctsk* (cathepsin K), *Car2* (carbonic anhydrase 2), *Mmp9* (matrix metalloproteinase 9), and *Calcr* (calcitonin receptor). However, *Marco*, a macrophage receptor, was not reduced in the $Fos^{-/-}$ culture (Table I).

TABLE I
Identification of c-Fos target genes by transcriptional profiling
ΔNFAT/GFP, -fold increase between ΔNFAT- and GFP-expressing $Fos^{-/-}$ splenocytes in osteoclastogenic cultures. A, absent; NC, no change.

Accession No.	Gene	Sp+/+	Sp−/−	Bm+/+	ΔNFAT/GFP
M99054	*Acp5*	3836	462	2580	4.0
AJ006033	*Ctsk*	2862	61	2495	8.4
M25944	*Car2*	971	14	719	3.2
AF087434	*Nfatc1*	752	A	325	3.5
U69535	*Sema4d*	707	A	309	2.0
AV239570	*Mmp9*	620	80	451	NC
AA656014	*Tm7sf*	593	30	295	NC
AW125713	Unknown	544	60	331	NC
U87814	*Pstpip1*	528	A	207	NC
AV251613	Unknown	357	A	120	6.5
U18542	*Calcr*	337	A	395	12.2
X53929	*Dcn*	320	A	321	NC
L22545	*Col18a1*	254	A	188	7.4
AF029215	Antigen for MRC OX-2	214	A	111	2.7
AF042487	*Kcnn4*	208	A	117	NC
U18424	*Marco*	108	761	223	NC

To confirm the differential expression at the protein level, Western blot analysis was performed using total protein extracts prepared on day 6 from the osteoclastogenic co-cultures. Consistent with the RNA data, NFATc1 was not detectable in the $Fos^{-/-}$ culture (Fig. 1*A*). The size variation of NFATc1 in the wild-type bone marrow culture may be caused by either degradation products or by different isoforms of NFATc1 (26, 27). Next we examined the subcellular localization of NFATc1 in mature osteoclasts freshly isolated from the femurs of wild-type mice. Immunofluorescence microscopy showed nuclear staining of NFATc1 but not NFATc2 in mature multinucleated osteoclasts generated *in vivo* (Fig. 1*B*). Western blot analysis of nuclear extracts from the macrophage-osteoclast precursor RAW264.7 cells demonstrated that nuclear NFATc1 was detectable only after RANKL stimulation (Fig. 1*C*). These data suggest that RANKL stimulates NFATc1 synthesis via c-Fos.

c-Fos Binds to the Nfatc1 Promoter—Putative c-Fos binding sites have been mapped in the promoter region of *Nfatc1* (Fig. 2*A*) (27, 28). To examine whether the *Nfatc1* promoter could be directly regulated by c-Fos in osteoclast precursors, we performed a chromatin immunoprecipitation assay using primary wild-type bone marrow cells and $Fos^{-/-}$ splenocytes treated with RANKL. The *Nfatc1*-P1 promoter fragment containing the distal block of homology between human and mouse sequences (27) was specifically precipitated with an anti-c-Fos antibody in samples prepared from wild-type cells treated with RANKL (Fig. 2*B*). The proximal block of homology could not be analyzed because of difficulty in PCR amplification. We also tested whether the *Acp5* promoter (Fig. 3*A*) was precipitated by anti-c-Fos antibody (Fig. 2*B*). In wild-type cells, c-Fos is present on the *Acp5* promoter in the absence of RANKL, and c-Fos occupancy of the *Acp5* promoter increases after RANKL treatment.

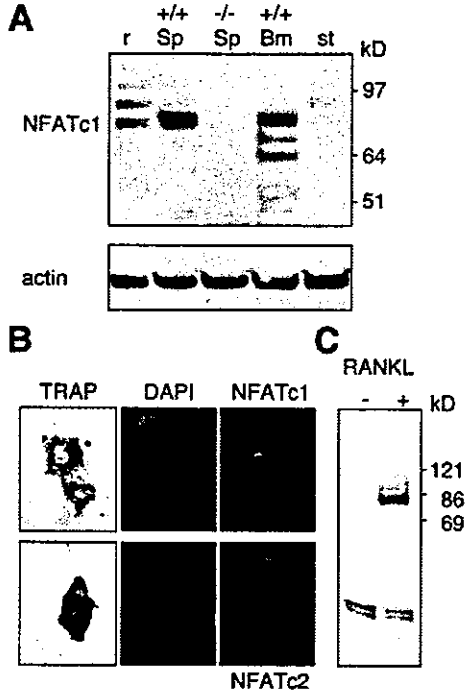

FIG. 1. **Expression of NFATc1.** *A*, NFATc1 is undetectable by Western blotting in $Fos^{-/-}$ osteoclastogenic culture. Splenocytes (*Sp*) and bone marrow cells (*Bm*) were co-cultured with ST2-T cells (*st*) for 6 days under osteoclastogenic conditions. Protein extracts *in toto* were analyzed using anti-NFATc1 monoclonal antibody (7A6). +/+ and −/− indicate wild-type and $Fos^{-/-}$ cultures, respectively. *r*, positive control Ramos cell extract. *B*, nuclear localization of NFATc1 in freshly isolated mature multinucleated osteoclasts. Immunofluorescence microscopy was performed with the anti-NFATc1 and anti-NFATc2 (G1-D10) antibodies. *TRAP*, TRAP activity stain; *DAPI*, 4′,6-diamidino-2-phenylindole (a nuclear stain). Note that the NFATc2-positive cell is TRAP-negative. *C*, Western blot analysis of nuclear extracts prepared from RAW264.7 cells cultured in the absence (−) or presence (+) of RANKL for 4 days using the anti-NFATc1 antibody.

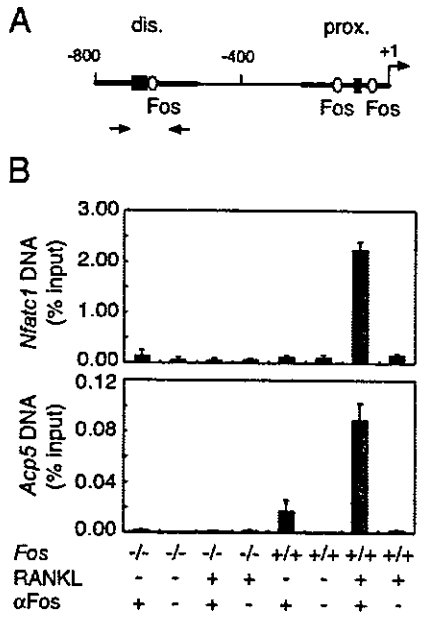

FIG. 2. **c-Fos binds to the *Nfatc1* promoter.** *A*, schematic presentation of putative Fos (*open ovals*) and NFAT (*closed rectangles*) binding sites in the mouse *Nfatc1* promoter (27, 28). The numbering is relative to the proximal transcriptional start site directed by promoter P1. Distal (*dis.*) and proximal (*prox.*) blocks of homology are shown in *thick lines*. *Arrows*, PCR primers. *B*, chromatin immunoprecipitation assay. Non-adherent $Fos^{-/-}$ splenocytes and wild-type bone marrow cells were treated with or without RANKL for 20 h before cross-linking. Precipitation was performed with IgG or anti-c-Fos antibody (*αFos*), and the amounts of precipitated DNA relative to total input DNA were quantified by a real-time PCR for *Nfatc1* (*top*) and *Acp5* (*bottom*; see Fig. 3*A* for PCR primers).

These results suggest that c-Fos binds to the *NFATc1* and *Acp5* promoters during osteoclastogenesis.

Acp5 and Calcr Promoters Contain Functional NFAT/AP-1 Sites—It is known that AP-1 composed of Fos/Jun dimers and NFAT transcription factors can cooperatively bind to promoter regions of various genes including the IL-2 gene (29, 30). To study the molecular mechanisms by which NFAT is involved in the regulation of osteoclast-specific gene expression we examined promoter sequences of *Acp5* and *Calcr*, two potential c-Fos target genes (Table I). First we searched for such composite binding sites for NFAT and AP-1 (NFAT/AP-1 sites) in mouse, human, and pig *Acp5* promoter sequences. Two short stretches were highly conserved around the multiple transcription start sites, which we termed *Acp5*-160 and *Acp5*-120, respectively (*Acp5* elements located at −160 and −120 relative to the 3′ end of exon 1). Sequences of the conserved *Acp5*-120 were found to be similar to the prototypical 15-bp NFAT/AP-1 site in the IL-2 promoter (15) (Fig. 3*A*). *Acp5*-160 contains the binding site for the microphthalmia transcription factor (31). From EMSA results, the binding activity at *Acp5*-120 was indistinguishable from that observed with the IL-2 site (Fig. 3*B*). Binding of c-Fos to the *Acp5* promoter in osteoclasts was demonstrated by chromatin immunoprecipitation assay (Fig. 2*B*). Then we mutated the putative NFAT site in *Acp5*-120 from GGAGAA to GGCCCG in *Acp5*-luciferase reporter plasmids. Both human and mouse wild-type *Acp5*-luciferase constructs were most efficiently activated with NFATc4 compared with NFATc1, NFATc2, and NFATc3 in transient transfection assays (data not shown). Thus we constructed a constitutively active nuclear form of NFATc4, ΔNFAT (20), fused to GFP. When the wild-type and mutant reporter plasmids were co-transfected with a ΔNFAT expression plasmid into RAW264.7 cells, ΔNFAT activated the wild-type *Acp5* promoter more efficiently than the mutant promoter (Fig. 3*C*). Furthermore, the *Acp5* promoter activity was enhanced by a co-transfected c-Fos expression vector and suppressed by small interfering RNA vectors for c-Fos in transient transfection assays (Fig. 3*D*). These data suggest that *Acp5*-120 is a functional NFAT/AP-1 binding site in the *Acp5* promoter.

Next we searched for NFAT/AP-1 sites in the mouse osteoclast-specific *Calcr*-P3 promoter (22) and found eight putative NFAT/AP-1 sites in the −797 *Calcr*-P3 promoter (Fig. 4*A*). Co-transfection of both the *Calcr*-P3-luciferase reporter plasmids and the ΔNFAT-expression vector into RAW264.7 cells resulted in a 30-fold increase in promoter activity above constitutive levels. Sequential 5′ deletion of the *Calcr*-P3 promoter demonstrated that the −178 construct containing the putative NFAT/AP-1 sites 1–4 was sufficient for full activity. Site-specific mutagenesis of each NFAT site from GGAAAN to GGCCCG revealed that site 2 at −93 was critical and that sites 1, 3, and 4 appear to cooperate with site 2 (Fig. 4*A*). In EMSA, site 2 was bound by NFATc1 using either RANKL-stimulated RAW264.7 nuclear extracts or *in vitro* translation products (Fig. 4*B*). Next we transfected RAW264.7 cells with *Calcr*-P3-luciferase reporters and treated them with the calcium ionophore A23187. We observed that the *Calcr* promoter activities were enhanced only when site 2 was present presumably

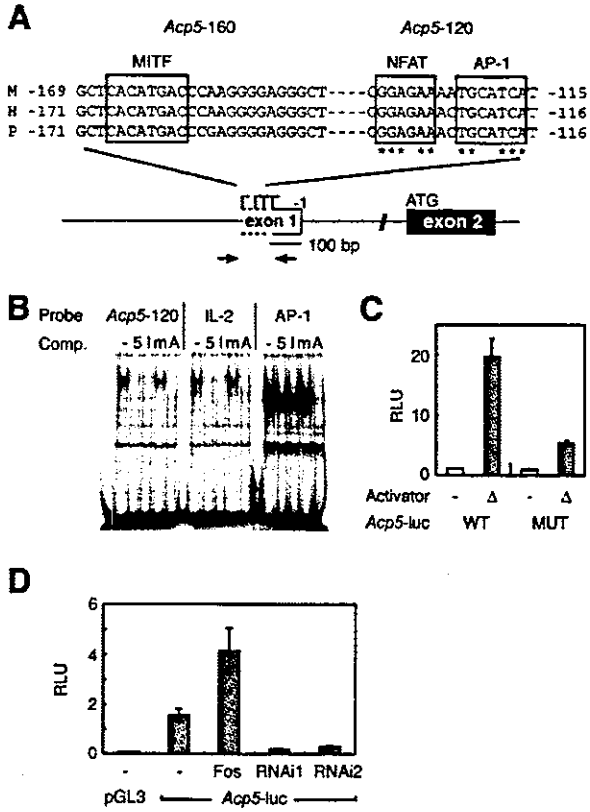

FIG. 3. **Identification of NFAT/AP-1 site in the *Acp5* promoter.** *A*, conserved *Acp5* promoter sequences in mouse (*M*), human (*H*), and pig (*P*). *Asterisks* indicate nucleotides identical to the 15-bp mouse IL-2 distal NFAT/AP-1 site. *Arrows* indicate PCR primers for the chromatin immunoprecipitation assay in Fig. 2*B*. *B*, EMSA using *Acp5*-120 (*5*), IL-2 distal NFAT/AP-1 site (*I*) and AP-1 consensus (*A*) or mutant (*m*) sites for probes and competitors (*Comp.*). Nuclear extracts containing NFAT binding activity were prepared from osteoclastogenic co-culture. *C*, transient transfection assay in RAW264.7 cells using wild-type (*WT*) and mutant (*MUT*) mouse *Acp5* promoter-luciferase constructs. The activator plasmid expressing ΔNFAT (Δ) was co-transfected. *RLU*, relative light units (normalized to co-transfected *Renilla* luciferase activity and relative to the unstimulated wild-type promoter). *D*, the *Acp5* promoter-luciferase construct was activated by c-Fos expression vector (*Fos*) and suppressed by Fos small interfering RNA vectors (*RNAi1*, *RNAi2*) in transient co-transfection in RAW264.7 cells.

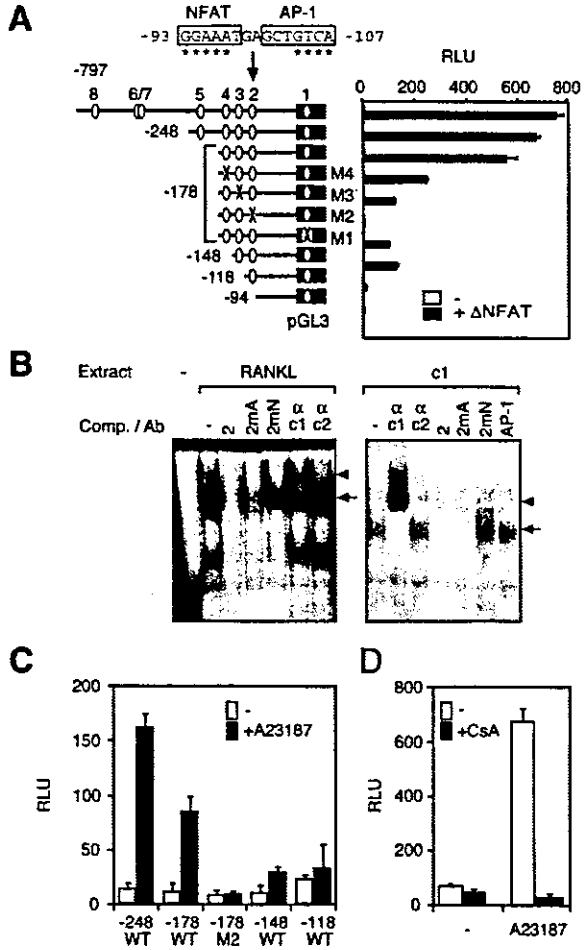

FIG. 4. **Identification of NFAT/AP-1 sites in the *Calcr*-P3 promoter.** *A*, a series of *Calcr*-P3 constructs was tested in RAW264.7 cells. The numbering is relative to the transcriptional start. *Open ovals* are sites 1–8 (22), and *X* is a site-specific mutant. *Asterisks* indicate nucleotides that are identical between *Calcr*-P3 site 2 and the IL-2 site. Relative light units (*RLU*) are normalized to micrograms of protein and are relative to unstimulated pGL3, a promoterless luciferase vector. *B*, EMSA using *Calcr*-P3 site 2. The DNA-binding protein source was either nuclear extracts prepared from RAW264.7 cells cultured in the absence (−) or presence of RANKL or *in vitro* translated NFATc1 (*c1*). *Arrows* and *arrowheads* indicate specific NFAT binding activity and supershifts, respectively. The oligonucleotide competitors were wild-type site 2 (*2*), site 2 with the putative AP-1 site mutated (*2mA*), site 2 with the NFAT site mutated (*2mN*), and wild-type AP-1 (*AP-1*). Supershifts were done with antibodies to NFATc1 (*αc1*) and NFATc2 (*αc2*). *C*, induction of *Calcr*-P3 by A23187 (1 μM), which was added to transfected RAW264.7 cells 2 h before harvest. *WT*, wild type. *D*, transient transfection assay in RAW264.7 cells using the −319 *Calcr*-P3-luciferase construct. Cyclosporin A (1 μg/ml) was added 1 h before transfection, and A23187 (1 μM) was added for 4 h before harvest.

through activation of endogenous NFAT (Fig. 4*C*). Furthermore, the stimulatory effect of A23187 was blunted by pretreatment of the cells with cyclosporin A (Fig. 4*D*). These data suggest that site 2 is the critical NFAT site in the *Calcr* promoter.

NFAT Rescues Osteoclast Differentiation in $Fos^{-/-}$ Precursors—To test whether NFAT activity could rescue osteoclastogenesis in the absence of c-Fos, we introduced GFP or the GFP fusion ΔNFAT into $Fos^{-/-}$ splenocytes by retroviral gene transfer. Infected cells were co-cultured with the ST2-T cells under osteoclastogenic conditions. At day 6, mRNA was harvested and microarray analysis was performed to compare gene expression between GFP and ΔNFAT virus-infected $Fos^{-/-}$ cells. Strikingly, expression of ΔNFAT activated about two-thirds of the genes that failed to be induced in $Fos^{-/-}$ cells including *Acp5*, *Calcr*, *Ctsk*, and endogenous *Nfatc1* (Table I, ΔNFAT/GFP). This indicated that the differentiation block was to a large extent overcome by ΔNFAT in the absence of c-Fos when RANKL from ST2-T cells was present. Indeed, whereas abundant GFP-positive cells were observed by day 6 with both viruses, TRAP-positive cells were generated only with ΔNFAT virus (Fig. 5*A*). Next we tested whether the ΔNFAT-expressing $Fos^{-/-}$ osteoclasts could resorb bone. Although resorption pits were not visible on bone slices in cultures of GFP virus-infected $Fos^{-/-}$ splenocytes, co-cultures containing ΔNFAT virus-infected $Fos^{-/-}$ cells generated multiple resorption pits (bone surface resorbed, 2.3 ± 0.5%) (Fig. 5*B*). Next we compared the rescue efficiency in two types of osteoclastogenic cultures, co-culture using ST2-T cells and osteoblast-free cultures using only soluble M-CSF and RANKL. In co-cultures, the rescue with ΔNFAT was comparable with that with c-Fos as judged by

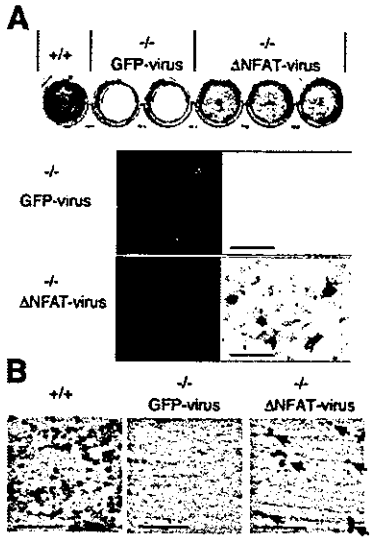

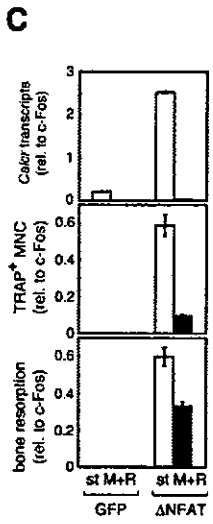

FIG. 5. **Rescue of osteoclast formation with ΔNFAT.** *A*, TRAP staining of osteoclastogenic co-cultures derived from wild-type (+/+) splenocytes and GFP and ΔNFAT virus-infected $Fos^{-/-}$ splenocytes (−/−). *Below*, GFP fluorescence and TRAP stain are shown in higher magnification. The *bars* represent 100 μm. *B*, bone resorption assay. Infected cells were co-cultured with ST2-T cells on bovine bone slices for 10 days, and pit formation was examined in a double-blind study with backscattered electron imaging. The *bars* represent 0.75 mm. *Arrows* indicate bone resorption pits. *C*, rescue activity of ΔNFAT virus relative to that of c-Fos virus. *st*, osteoclastogenic co-cultures using ST2-T cells. *M+R*, osteoblast-free cultures using soluble M-CSF and RANKL. $Fos^{-/-}$ splenocytes were infected with GFP, c-Fos, or ΔNFAT viruses. *Calcr* transcripts were quantitated by real-time PCR; TRAP-positive multinucleated cells (*MNC*) were counted, and the resorbed area (%) was measured on bone surfaces.

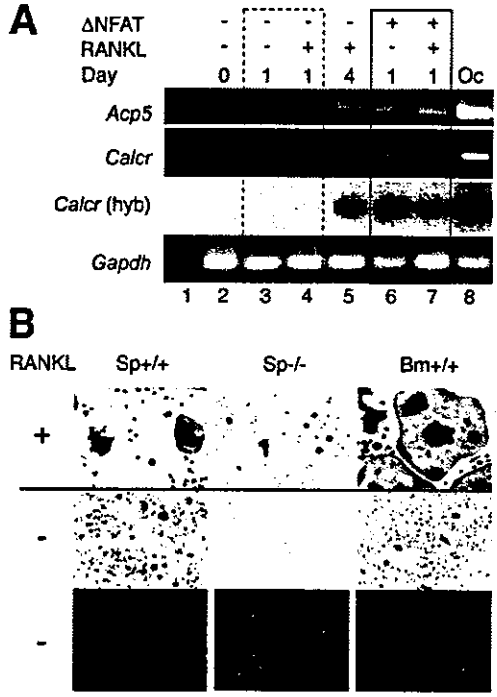

FIG. 6. **Rescue of osteoclast formation with ΔNFAT in the absence of RANKL.** *A*, transient transfection of ΔNFAT-expression vector induces endogenous *Acp5* and *Calcr* expression in RAW264.7 cells untreated or treated with 30 ng/ml RANKL as indicated and harvested at the days depicted. Osteoclasts generated in co-culture served as positive control (*lane 8*) and no RNA as negative control (*lane 1*). Transcripts were analyzed by reverse transcriptase-PCR with primers for *Acp5*, *Calcr* (all isoforms), and glyceraldehyde-3-phosphate dehydrogenase (*Gapdh*). The reverse transcripts-PCR products for *Calcr* were also detected by hybridization with an internal probe (*hyb*). *B*, rescue of TRAP-positive $Fos^{-/-}$ cells by ΔNFAT requires RANKL. M-CSF-dependent macrophages derived from wild-type and $Fos^{-/-}$ splenocytes (*Sp+/+* and *Sp−/−*) and wild-type bone marrow cells (*Bm+/+*) were infected with the GFP ΔNFAT virus and then were cultured for 3 more days in the presence or absence of RANKL. The *bottom row* shows expression of GFP ΔNFAT fusion protein.

Calcr expression, TRAP-positive cell numbers, and resorption (Fig. 5*C*, *st*). In contrast, in the absence of stromal cells the rescue with ΔNFAT was lower than that of c-Fos based on all three parameters (Fig. 5*C*, *M+R*). Apart from the differences in efficiency in both cultures, ΔNFAT substituted at least in part for the osteoclastogenic function of c-Fos to the extent that $Fos^{-/-}$ splenocytes formed bone resorption pits in the presence of RANKL. In addition, gene transfer of the human full-length *NFATc1* also rescued $Fos^{-/-}$ osteoclastogenesis *in vitro* (data not shown). These data collectively indicate that the lack of NFATc1 is a major reason for the differentiation block in $Fos^{-/-}$ osteoclast precursors.

NFAT Rescue of $Fos^{-/-}$ Precursors Is RANKL-dependent—To examine the role of RANKL in NFAT-induced osteoclast formation, we introduced the GFP fusion ΔNFAT into RAW264.7 cells by transient transfection. This resulted in the induction of the endogenous *Acp5* and *Calcr* genes as early as 1 day after transfection even in the absence of RANKL (Fig. 6*A*). This is consistent with the reported osteoclastogenic activity of NFATc1 in the absence of RANKL (5). Next, we tested whether ΔNFAT could rescue $Fos^{-/-}$ precursors in the absence of RANKL. ΔNFAT produced bone-resorbing TRAP-positive cells from wild-type precursors (*Bm+/+*, *Sp+/+*) in the absence or presence of RANKL (Fig. 6*B*). However, $Fos^{-/-}$ precursors (*Sp−/−*) hardly produced any TRAP-positive cells upon introduction of ΔNFAT in the absence of RANKL (Fig. 6*B*), and no bone resorption pits were observed (data not shown). These data suggest that the rescue of $Fos^{-/-}$ cells with NFAT activity requires receptor activator of NF-κB (RANK) signaling.

DISCUSSION

It has been established that the lack of c-Fos expression results in a differentiation block in the osteoclast lineage (7–9). However, whether this is a cumulative effect of numerous deregulated c-Fos target genes or an effect of one critical c-Fos target gene is unclear. Our results show that the absence of *Nfatc1* expression in $Fos^{-/-}$ precursors is the major cause of the differentiation block because an active form of NFAT alone rescued osteoclast-specific gene expression and bone resorptive function.

We have identified NFAT/AP-1 sites in the *Acp5* and *Calcr* promoters. EMSA showed that NFAT and AP-1 cooperatively bind to the *Acp5* NFAT/AP-1 site, and the chromatin immunoprecipitation assay indicated that c-Fos binds to the *Acp5* promoter in osteoclasts. These observations are consistent with the idea that NFATc1 and c-Fos synergize to activate the *Acp5* promoter (5). On the other hand, the rescue of osteoclastogenesis by ΔNFAT alone in the absence of c-Fos clearly demonstrates that c-Fos is not essential for activation of the *Acp5* promoter. To activate these promoters in $Fos^{-/-}$ precursors, ΔNFAT may interact with Jun-Jun homodimers (32) or may act alone in the absence of cooperative partners (33). EMSA using $Fos^{-/-}$ cell extract in combination with *in vitro* translated NFATc1 will help to address this issue. Although binding of

NFAT to the *Calcr* promoter was unambiguously demonstrated by EMSA, binding of AP-1 to the *Calcr* promoter needs to be rigorously tested in the future.

Importantly, osteoclast-specific gene expression is not entirely rescued with ΔNFAT. Those genes for which expression is not rescued, for example *Mmp9*, may be more strictly dependent on c-Fos or additional c-Fos-dependent transcription factors. Curiously, the rescue activity of ΔNFAT was similar to that of c-Fos when $Fos^{-/-}$ precursors were co-cultured with ST-2 but was lower than that of c-Fos when soluble M-CSF and RANKL were used. Therefore, c-Fos dependence appears to increase as stromal factors decrease. One of the stromal factors involved might be the ligand of osteoclast-associated receptor (OSCAR) (34). Whereas in wild-type precursors ΔNFAT or NFATc1 induce osteoclast differentiation even in the absence of RANKL (5), ΔNFAT expression in $Fos^{-/-}$ precursors failed to rescue osteoclast differentiation in the absence of RANKL. This suggests that in the absence of RANKL, NFAT requires c-Fos, presumably as a binding partner or possibly indirectly to exert its osteoclastogenic function. It also suggests that RANKL may induce an alternative partner for NFAT that can substitute for c-Fos function in $Fos^{-/-}$ cells.

Taken together, these results demonstrate that a major function of c-Fos during osteoclast formation is to trigger a transcriptional regulatory cascade by producing and cooperating with NFATc1, thereby activating a number of target genes involved in osteoclast differentiation and function. These yet to be identified novel target genes together with *Nfatc1* may provide additional drug targets for bone diseases including osteoporosis and rheumatoid arthritis.

Acknowledgments—We thank H. Meguro for help with GeneChip analysis, T. Chambers for help with the preparation of mature osteoclasts, T. Sano for electron microscopy, H. Peng for technical assistance, G. D. Roodman for *Acp5*-luciferase constructs, T. Hoey and N. A. Clipstone for NFAT cDNAs, I. Graef and G. R. Crabtree for NFAT antibodies and cDNAs, R. Medzhitov for small interfering RNA vectors, M. Tsuri-Jinno for technical help, K. Ikeda, and P. E. Auron for support and discussions, and L. Bakiri, M. Sibilia, J.-P. David, and N. Ray for critical reading of the manuscript.

REFERENCES

1. Chinenov, Y., and Kerppola, T. K. (2001) *Oncogene* **20,** 2438–2452
2. Shaulian, E., and Karin, M. (2002) *Nat. Cell Biol.* **4,** E131–E136
3. Teitelbaum, S. L., and Ross, F. P. (2003) *Nat. Rev. Genet.* **4,** 638–649
4. Karsenty, G., and Wagner, E. F. (2002) *Dev. Cell* **2,** 389–406
5. Takayanagi, H., Kim, S., Koga, T., Nishina, H., Isshiki, M., Yoshida, H., Saiura, A., Isobe, M., Yokochi, T., Inoue, J., Wagner, E. F., Mak, T. W., Kodama, T., and Taniguchi, T. (2002) *Dev. Cell* **3,** 889–901
6. Komarova, S. V., Pilkington, M. F., Weidema, A. F., Dixon, S. J., and Sims, S. M. (2003) *J. Biol. Chem.* **278,** 8286–8293
7. Wang, Z. Q., Ovitt, C., Grigoriadis, A. E., Mohle-Steinlein, U., Ruther, U., and Wagner, E. F. (1992) *Nature* **360,** 741–744
8. Johnson, R. S., Spiegelman, B. M., and Papaioannou, V. (1992) *Cell* **71,** 577–586
9. Grigoriadis, A. E., Wang, Z. Q., Cecchini, M. G., Hofstetter, W., Felix, R., Fleisch, H. A., and Wagner, E. F. (1994) *Science* **266,** 443–448
10. Matsuo, K., Owens, J. M., Tonko, M., Elliott, C., Chambers, T. J., and Wagner, E. F. (2000) *Nat. Genet.* **24,** 184–187
11. Fleischmann, A., Hafezi, F., Elliott, C., Reme, C. E., Ruther, U., and Wagner, E. F. (2000) *Genes Dev.* **14,** 2695–2700
12. Takayanagi, H., Kim, S., Matsuo, K., Suzuki, H., Suzuki, T., Sato, K., Yokochi, T., Oda, H., Nakamura, K., Ida, N., Wagner, E. F., and Taniguchi, T. (2002) *Nature* **416,** 744–749
13. Hoey, T., Sun, Y. L., Williamson, K., and Xu, X. (1995) *Immunity* **2,** 461–472
14. Crabtree, G. R., and Olson, E. N. (2002) *Cell* **109,** (suppl.) S67–S79
15. Hogan, P. G., Chen, L., Nardone, J., and Rao, A. (2003) *Genes Dev.* **17,** 2205–2232
16. Ishida, N., Hayashi, K., Hoshijima, M., Ogawa, T., Koga, S., Miyatake, Y., Kumegawa, M., Kimura, T., and Takeya, T. (2002) *J. Biol. Chem.* **277,** 41147–41156
17. Hirotani, H., Tuohy, N. A., Woo, J.-T., Stern, P. H., and Clipstone, N. A. (2004) *J. Biol. Chem.* **279,** 13984–13992
18. Lean, J. M., Matsuo, K., Fox, S. W., Fuller, K., Gibson, F. M., Draycott, G., Wani, M. R., Bayley, K. E., Wong, B. R., Choi, Y., Wagner, E. F., and Chambers, T. J. (2000) *Bone* **27,** 29–40
19. Schreiber, E., Matthias, P., Muller, M. M., and Schaffner, W. (1989) *Nucleic Acids Res.* **17,** 6419
20. Molkentin, J. D., Lu, J. R., Antos, C. L., Markham, B., Richardson, J., Robbins, J., Grant, S. R., and Olson, E. N. (1998) *Cell* **93,** 215–228
21. Onishi, M., Kinoshita, S., Morikawa, Y., Shibuya, A., Phillips, J., Lanier, L. L., Gorman, D. M., Nolan, G. P., Miyajima, A., and Kitamura, T. (1996) *Exp. Hematol.* **24,** 324–329
22. Anusaksathien, O., Laplace, C., Li, X., Ren, Y., Peng, L., Goldring, S. R., and Galson, D. L. (2001) *J. Biol. Chem.* **276,** 22663–22674
23. Barton, G. M., and Medzhitov, R. (2002) *Proc. Natl. Acad. Sci. U. S. A.* **99,** 14943–14945
24. Weinmann, A. S., and Farnham, P. J. (2002) *Methods (Orlando)* **26,** 37–47
25. Lacey, D. L., Timms, E., Tan, H. L., Kelley, M. J., Dunstan, C. R., Burgess, T., Elliott, R., Colombero, A., Elliott, G., Scully, S., Hsu, H., Sullivan, J., Hawkins, N., Davy, E., Capparelli, C., Eli, A., Qian, Y. X., Kaufman, S., Sarosi, I., Shalhoub, V., Senaldi, G., Guo, J., Delaney, J., and Boyle, W. J. (1998) *Cell* **93,** 165–176
26. Sherman, M. A., Powell, D. R., Weiss, D. L., and Brown, M. A. (1999) *J. Immunol.* **162,** 2820–2828
27. Chuvpilo, S., Jankevics, E., Tyrsin, D., Akimzhanov, A., Moroz, D., Jha, M. K., Schulze-Luehrmann, J., Santner-Nanan, B., Feoktistova, E., Konig, T., Avots, A., Schmitt, E., Berberich-Siebelt, F., Schimpl, A., and Serfling, E. (2002) *Immunity* **16,** 881–895
28. Zhou, B., Cron, R. Q., Wu, B., Genin, A., Wang, Z., Liu, S., Robson, P., and Baldwin, H. S. (2002) *J. Biol. Chem.* **277,** 10704–10711
29. Chen, L., Glover, J. N., Hogan, P. G., Rao, A., and Harrison, S. C. (1998) *Nature* **392,** 42–48
30. Diebold, R. J., Rajaram, N., Leonard, D. A., and Kerppola, T. K. (1998) *Proc. Natl. Acad. Sci. U. S. A.* **95,** 7915–7920
31. Luchin, A., Suchting, S., Merson, T., Rosol, T. J., Hume, D. A., Cassady, A. I., and Ostrowski, M. C. (2001) *J. Biol. Chem.* **276,** 36703–36710
32. Macian, F., Lopez-Rodriguez, C., and Rao, A. (2001) *Oncogene* **20,** 2476–2489
33. Stroud, J. C., and Chen, L. (2003) *J. Mol. Biol.* **334,** 1009–1022
34. Kim, N., Takami, M., Rho, J., Josien, R., and Choi, Y. (2002) *J. Exp. Med.* **195,** 201–209

[CANCER RESEARCH 64, 2418–2423, April 1, 2004]

Identification of Soluble NH_2-Terminal Fragment of Glypican-3 as a Serological Marker for Early-Stage Hepatocellular Carcinoma

Yoshitaka Hippo,[1] Kiyotaka Watanabe,[4] Akira Watanabe,[1] Yutaka Midorikawa,[5] Shogo Yamamoto,[2] Sigeo Ihara,[2] Susumu Tokita,[7] Hiroko Iwanari,[7] Yukio Ito,[7] Kiyotaka Nakano,[6] Jun-ichi Nezu,[6] Hiroyuki Tsunoda,[6] Takeshi Yoshino,[6] Iwao Ohizumi,[6] Masayuki Tsuchiya,[6] Shin Ohnishi,[4] Masatoshi Makuuchi,[5] Takao Hamakubo,[3] Tatsuhiko Kodama,[3] and Hiroyuki Aburatani[1]

[1]Genome Science Division, [2]Division of Dynamical Bioinformatics, and [3]Division of Molecular Biology and Medicine, Research Center for Advanced Science and Technology, The University of Tokyo, Tokyo, Japan; Departments of [4]Gastroenterology and [5]Hepato-Biliary-Pancreatic Surgery, Graduate School of Medicine, The University of Tokyo, Tokyo, Japan; [6]Chugai Pharmaceutical Co., Ltd., Shizuoka, Japan; and [7]Perseus Proteomics, Inc., Tokyo, Japan

ABSTRACT

For detection of hepatocellular carcinoma (HCC) in patients with liver cirrhosis, serum α-fetoprotein has been widely used, but its sensitivity has not been satisfactory, especially in small, well-differentiated HCC, and complementary serum marker has been clinically required. Glypican-3 (GPC3), a heparan sulfate proteoglycan anchored to the plasma membrane, is a good candidate marker of HCC because it is an oncofetal protein overexpressed in HCC at both the mRNA and protein levels. In this study, we demonstrated that its NH_2-terminal portion [soluble GPC3 (sGPC3)] is cleaved between Arg^{358} and Ser^{359} of GPC3 and that sGPC3 can be specifically detected in the sera of patients with HCC. Serum levels of sGPC3 were 4.84 ± 8.91 ng/ml in HCC, significantly higher than the levels seen in liver cirrhosis (1.09 ± 0.74 ng/ml; $P < 0.01$) and healthy controls (0.65 ± 0.32 ng/ml; $P < 0.001$). In well- or moderately-differentiated HCC, sGPC3 was superior to α-fetoprotein in sensitivity, and a combination measurement of both markers improved overall sensitivity from 50% to 72%. These results indicate that sGPC3 is a novel serological marker essential for the early detection of HCC.

INTRODUCTION

Hepatocellular carcinoma (HCC) is one of the most prevalent cancers worldwide, and its incidence is still increasing (1). Because HCC develops from cirrhotic liver after chronic infection with hepatitis virus B or C, patients with liver cirrhosis (LC) are advised to undergo periodical screening of serum α-fetoprotein (AFP) levels and liver ultrasound for the purpose of early detection of cancer (2). AFP is a glycoprotein expressed abundantly in fetal liver but not in normal adult liver and is re-expressed by HCC as it dedifferentiates from a premalignant lesion in the cirrhotic liver through well-differentiated (WD) and moderately differentiated (MD) HCC to poorly differentiated HCC (3). AFP has been used as a serum marker of HCC for more than 40 years. However, ultrasound imaging has been more effective lately in early detection of small WD HCC, in which AFP has yet to be elevated (4), highlighting the clinical need for novel sensitive serum markers for WD HCC.

Many previous studies have identified genes up-regulated in HCC compared with surrounding noncancerous lesions using differential display or cDNA subtraction (5–8). Recently, microarray studies on HCC presented gene lists containing a number of overexpressed genes (9–14). However, to determine whether a gene is a good candidate as a serological marker of WD HCC, it is crucial to determine the following: (*a*) whether it is overexpressed in WD HCC; (*b*) whether it is not expressed abundantly in other normal organs; and (*c*) whether it is detectable in the serum.

Overexpression of *GPC3* mRNA in HCC has been reported by ourselves and several other groups (15–18). Moreover, frequency of *GPC3* mRNA overexpression was significantly higher than that of elevated serum level and mRNA level of AFP in small HCC (16). We also observed frequent overexpression of *GPC3* in WD HCC compared with AFP with microarray analysis.[8] Together with minimal expression in normal organs (16, 19), GPC3 has, undoubtedly, previously existed as an attractive candidate marker of HCC. We showed previously using a monoclonal antibody (mAb) that GPC3 protein is also highly expressed in HCC (15). In this study, we further characterized GPC3 protein using a panel of newly generated mAbs and investigated whether it could be detected specifically in the sera of the patients with HCC. Finally, we successfully established a detection system for the soluble fragment of GPC3 (sGPC3) and confirmed its usefulness as a novel biomarker for HCC.

MATERIALS AND METHODS

Serum Samples. Serum samples were collected at Tokyo University Hospital with informed consent from 69 patients with HCC and 38 patients with LC, defined according to the following criteria: patients with a pathological diagnosis of HCC after surgery or with evidence of tumor stain on computed tomography or angiography were diagnosed with HCC; and patients diagnosed with LC were limited to those who had no history of HCC and no ultrasound evidence of tumor for more than 6 months from the day of serum collection.

Purification of Recombinant GPC3 Proteins. For protein expression, we used modified pCXN vector that contained dihydrofolate reductase expression unit as a selection marker. Original pCXN vector (20) was generously provided by J. Miyazaki (Osaka University Medical School, Osaka, Japan). An expression vector for GPC3 that lacks the COOH-terminal hydrophobic glycosylated phosphatidylinositol (GPI)-anchoring domain, GPC3ΔGPI, was constructed by introducing cDNA corresponding to amino acid residues 1–563 of GPC3 into modified pCXN with a FLAG tag added at the COOH terminus. An expression vector for GPC3ΔGPI without heparan sulfate, GPC3ΔGPIΔHS, was constructed by changing Ser^{495} and Ser^{509} to Ala to abolish the heparan sulfate attachment site. These constructs were stably transfected into Chinese hamster ovary cells deficient in the dihydrofolate reductase gene. Culture media containing GPC3ΔGPI-FLAG or GPC3ΔGPIΔHS-FLAG recombinant proteins were collected and loaded to DEAE ion-exchange chromatography DEAE Sepharose FF (Amersham Bioscience, Tokyo, Japan). After washing, eluted protein solutions were applied to anti-FLAG M2 antibody beads (Sigma, St.

Received 7/19/03; revised 11/25/03; accepted 1/12/04.

Grant support: Grants-in-Aid for Scientific Research (B) 12557051 and 13218019 and Scientific Research on Priority Areas (C) 12217031 from the Ministry of Education, Culture, Sports, Science and Technology; Health and Labor Sciences Research Grants for Research on Hepatitis and BSE from the Ministry of Health Labor and Welfare; and funds from Uehara Memorial Foundation (H. Aburatani). This study was carried out as a part of The Technology Development for Analysis of Protein Expression and Interaction in Bioconsortia on R&D of New Industrial Science and Technology Frontiers that was overseen by the Industrial Science, Technology and Environmental Policy Bureau, Ministry of Economy, Trade and Industry and delegated to New Energy Development Organization.

The costs of publication of this article were defrayed in part by the payment of page charges. This article must therefore be hereby marked *advertisement* in accordance with 18 U.S.C. Section 1734 solely to indicate this fact.

Requests for reprints: Hiroyuki Aburatani, Genome Science Division, Research Center for Advanced Science and Technology, The University of Tokyo, 4-6-1 Komaba, Meguro-ku, Tokyo 153-8904, Japan. Phone: 81-3-5452-5235; Fax: 81-3-5452-5355; E-mail: haburata-tky@umin.ac.jp.

[8] Y. Midorikawa, S. Tsutsumi, K. Nishimura, N. Kamimura, M. Kano, H. Sakamoto, M. Makuuchi, and H. Aburatani. Transcriptional Signature in Progression of Hepatocellular Carcinoma, manuscript in preparation.

Louis, MO). Proteins eluted with solution containing 200 μg/ml FLAG peptide (Sigma) were subjected to gel filtration chromatography with HiLoad 26/60 Superdex200pg (Amersham Bioscience). Finally, recombinant protein was concentrated using DEAE Sepharose FF.

Generation of Anti-GPC3 mAbs. We used recombinant GPC3ΔGPI as an immunogen. Spleen cells were isolated and fused with mouse myeloma P3-X63Ag8U1 cells (American Type Culture Collection, Manassas, VA). Hybridomas were selected by ELISA against the purified recombinant GPC3ΔGPIΔHS-FLAG, followed by cloning with limited dilution. Three mouse mAbs (A1836A, M18D04, and M19B11) were used in this study. For epitope mapping of these mAbs, a pGEX-5X (Amersham Biosciences) construct for the NH_2-terminal portion of GPC3 (amino acids 25–358) was expressed in *Escherichia coli* BL21 Codon Plus (DE3) pLys (Stratagene, La Jolla, CA) as a glutathione *S*-transferase-fusion protein and subject to immunoblotting analysis.

Immunoblotting. Total cell lysates were obtained after lysis in 10 mM Tris (pH 7.4), 150 mM NaCl, 5 mM EDTA, 1.0% Triton X-100, 1.0% sodium deoxycholate, and 0.1% SDS with protease inhibitor mixture (Sigma). Culture supernatant was obtained from serum-free medium used for culture of hepatoma cells. Proteins were separated with 12% SDS-PAGE and transferred to polyvinylidene difluoride Hybond P membrane (Amersham Biosciences). The membrane was treated with 2% nonfat milk in TBS containing 0.05% Tween 20 (TBST) followed by incubation with anti-GPC3 mAb in TBST and subsequent incubation with horseradish peroxidase-conjugated secondary antibody (dilution, 1:5000; Amersham Biosciences) in TBST. The protein was visualized using the enhanced chemiluminescence plus detection system (Amersham Biosciences).

Immunoprecipitation. We first prepared antibody beads by covalently linking 25 μl of protein G-Sepharose (Amersham Biosciences) and 50 μg of anti-GPC3 mAb M18D04 or M19B11 with 20 mM dimethyl pimelimidate (ICN Aurora, Aurora, OH). We then added 50 μl of sera from the patients or culture media of HuH7 cells diluted in 250 μl with PBS to 25 μl of antibody beads and incubated them for 2 h at 4°C. After extensive washing with PBS, antibody beads were boiled for 5 min in 50 μl of SDS-PAGE loading buffer containing 10% 2-mercaptoethanol, and subsequently, immunoblotting was performed.

Sandwich ELISA. One μg of anti-GPC3 mAb A1836A per well was immobilized to 96-well plate Maxisorp (Nalge Nunc International, Roskilde, Denmark) and stabilized with Immunoassay Stabilizer (Advanced Biotechnologies Inc., Columbia, MD). Twenty-five μl of sera or standard were diluted with 100 μl of buffer containing 20% normal rabbit serum (Pel-Freez Biologicals, Rogers, AR), 1% BSA (Oriental Yeast Co., Ltd., Osaka, Japan), and 2% mouse ascites Hyb-3423 (Institute of Immunology, Tokyo, Japan) in 50 mM Tris-Cl (pH 8.0), 0.15 M NaCl, and 1 mM EDTA and incubated at room temperature for 2 h. After washing, 25 μl of biotinylated antibody solution containing anti-GPC3 mAbs M18D04 (1.88 μg/ml) and M19B11 (3.75 μg/ml) and 100 μl of horseradish peroxidase-labeled streptavidin (Vector Laboratories Inc., Burlingame, CA) were added to the plate and incubated twice at room temperature for 30 min. TMB Soluble Reagent and Stop Buffer (Scy Tek Laboratories, Inc., Logan, UT) were added as substrate, and absorbance at 450 nm was read with EIA Reader (Corona Electric Co., Ltd., Ibaraki, Japan). Recombinant GPC3ΔGPI was used as a standard sample in each assay.

Amino Acid Sequence Analysis. Recombinant GPC3ΔGPI and GPC3ΔGPIΔHS were purified and separated by SDS-PAGE and transferred to polyvinylidene difluoride membrane ProBlott (Applied Biosystems, Foster City, CA). The membrane was stained with CBB R-250, and sections containing bands of M_r 40,000 and M_r 30,000 were cut out separately. These polyvinylidene difluoride membrane sections were washed with a solution including 50% acetonitrile and 0.1% trifluoroacetic acid and applied to an ABI 492 Protein Sequencer (Applied Biosystems) to sequence the NH_2 terminus of the protein. Because the NH_2 terminus of the M_r 40,000 protein was blocked, the membrane was further incubated in acetate with 0.6 mg/ml 3-bromo-3-methyl-2-nitrophenyl-mecapto-3*H*-indole (ICN Biomedicals Inc., Irvine, CA) at 80°C for 1 h in the dark to chemically cleave the protein at the COOH terminus of tryptophan residues. After washing twice with 80% acetate and once with 10% methanol, the peptide was analyzed using an ABI 492 Protein Sequencer. The detected sequence was aligned using FASTS software available online,[9] and the protein was identified.

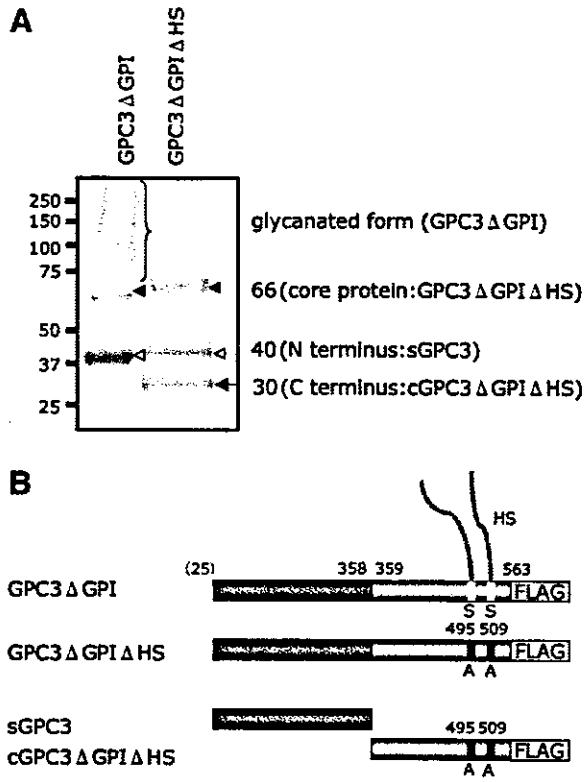

Fig. 1. Characterization of recombinant glypican-3 (GPC3) proteins. *A*, CBB R-250-stained SDS-PAGE of purified recombinant GPC3. *Brace*, glycanated GPC3 (smearing), GPC3ΔGPI; *closed arrowhead*, core protein of GPC3 (M_r 66,000) that lacks heparan sulfate glycosaminoglycan, GPC3ΔGPIΔHS; *open arrowhead*, sGPC3 (M_r 40,000); *arrow*, cGPC3ΔGPIΔHS (M_r 30,000). *B*, schematic diagram of recombinant proteins. *Numbers above the boxes* indicate amino acid residue number. Note that NH_2-terminal residue 25 is putative and indicated in *parentheses*. *HS*, heparan sulfate glycosaminoglycan.

RESULTS

The NH_2-Terminal Portion of GPC3 Is Cleaved between Arg^{358} and Ser^{359} *in Vitro*. We have previously generated mAb K6534 raised against a peptide corresponding to amino acids 355–371 of GPC3 protein, and we demonstrated, for the first time, overexpression of its core protein in HCC with immunoblotting using this antibody (15). Another antibody is required to construct a sandwich ELISA system for serum examination of GPC3, so we started generating high-affinity mAbs using recombinant GPC3ΔGPI as an immunogen. While purifying the immunogen from the culture supernatant of Chinese hamster ovary cells, we observed a M_r 40,000 band (Fig. 1*A*) in addition to the M_r 66,000 band that corresponds to core protein of GPC3 as observed with K6534 (15).

Because the NH_2 terminus of this M_r 40,000 band was modified, as revealed by initial amino acid sequencing, we performed sequencing of internal amino acids of the band after cleavage at the COOH terminus of tryptophan residues to verify its origin. We detected six cycles of three amino acid residues VRY, EPX, YES, ITY, LPX, and QSV, each cycle corresponding to the first to sixth residue following tryptophan (W), respectively. After alignment with FASTF algorithm, these sequences matched with the (W)VPETPV (amino acid 51–57), (W)YCSYCQ (amino acid 261–267), and (W)REYILS (amino acid

[9] http://fasta.bioch.virginia.edu/.

296–302) partial sequences of GPC3, respectively, indicating that this band is derived from an NH_2-terminal portion of GPC3. We designated this soluble cleaved fragment of GPC3 as sGPC3.

To further characterize sGPC3, we next tried to precisely identify the undetermined cleavage site by sequencing the residual COOH-terminal portion of GPC3 (designated cGPC3). However, the corresponding band was not visible by SDS-PAGE, presumably due to attachment of heparan sulfate glycosaminoglycan, leading to smearing (Fig. 1*A*). After substituting the two heparan sulfate attachment sites of the expression construct and purifying the resultant GPC3ΔGPIΔHS, we could observe a band of M_r 30,000, as expected (Fig. 1*A*). The NH_2-terminal sequence of this band was identified as SAYYPEDLF, identical to amino acids 359–367 of GPC3. Thus, the cleavage site was identified as being between Arg^{358} and Ser^{359} (Fig. 1*B*). We do not have precise information on the NH_2-terminal sequence of sGPC3 due to modification, but considering that amino acid 1–24 is a putative signal sequence, sGPC3 is likely to consist of amino acids 25–358 with an estimated molecular weight of 38,100, consistent with the M_r 40,000 band observed in SDS-PAGE (Fig. 1*A*).

Soluble GPC3 Is a Major Form of GPC3 Specifically Detected in the Sera of Patients with HCC. We succeeded in generating a number of high-affinity mAbs specific for GPC3 and classified these antibodies into two groups, N-mAbs and C-mAbs, according to their epitopes within amino acids 25–358 or 359–563, respectively (data not shown). These antibodies could also recognize endogenous GPC3 protein in immunoblotting: core protein (M_r 66,000) and glycanated form (smearing) of GPC3 were detected by both N-mAbs and C-mAbs; whereas sGPC3 (M_r 40,000) was detected only by N-mAbs (Fig. 2*A*). An additional M_r 50,000 band was detected strongly in the cell lysate of HepG2 with both N-mAbs and C-mAbs (Fig. 2*A*). This band was only weakly detectable in HuH6 cells and was undetectable in five other hepatoma cell lines (Fig. 2, *A* and *C*; data not shown), suggesting cell-specific variations in the processing of the protein. In the culture supernatant, sGPC3, rather than a core protein or a glycanated form of GPC3, was the major form of GPC3 detected (Fig. 2*A*).

Based on the above *in vitro* finding, we speculated that sGPC3, instead of core protein of GPC3, might be the major form of GPC3 in the sera of HCC patients. To avoid possible interference on immunoblotting by significant migration of albumin or immunoglobulin in the serum, we performed immunoprecipitation before immunoblottng using three N-mAbs (Fig. 2*B*). sGPC3 alone was successfully detected by immunoprecipitation with M18D04 (Fig. 2*C*) or M19B11 (data not shown) followed by immunoblotting with A1836A in the sera of patients with HCC, but not in sera from normal liver (NL). These results clearly demonstrate that sGPC3 is the major diagnostic target specifically detectable in the sera of HCC patients.

Soluble GPC3 Is Useful as a Serological Marker of WD HCC and MD HCC. We next constructed a sandwich ELISA system with these three antibodies to measure the serum level of sGPC3 (Fig. 3*A*). To verify the specificity of the assay, we performed immunoblotting of 10 sera samples from HCC with sGPC3 levels ranging from 4.0 to 55.0 ng/ml and 3 samples from NL with sGPC3 levels of <0.1 mg/ml. We detected only sGPC3 in all 10 HCC samples, whereas no band was detected in 3 samples from NL, indicating high sensitivity and specificity of the assay (Fig. 3*B*). When we examined sera from 69 cases with HCC, 38 cases with LC, and 96 cases with NL, the level of sGPC3 (mean ± SD) was 4.84 ± 8.91 ng/ml for HCC, 1.09 ± 0.74 ng/ml for LC, and 0.65 ± 0.32 ng/ml for NL and was significantly higher in HCC than in NL ($P < 0.001$, Student's t test) or in LC ($P < 0.01$; Fig. 3*C*).

We then evaluated sGPC3 as a general marker for HCC in comparison with AFP. Initial analysis of the receiver-operating characteristic curve using the data from 69 cases with HCC and 38 cases with LC suggested that, used in isolation, sGPC3 is not as good as AFP: the calculated area under the receiver-operating characteristic curve was 0.729 for sGPC3 and 0.799 for AFP (Fig. 3*D*). The sensitivity and specificity of sGPC3 for the diagnosis of HCC (cutoff value, 2.0 ng/ml) were 51% and 90%, respectively, whereas those of AFP measured in parallel (cutoff value, 20 ng/ml) were 55% and 90%, respectively. AFP and sGPC3 were not correlated ($r = 0.13$), and combination measurement of both markers markedly improved sensitivity to 72%.

HCC may be divided into two subgroups correlating to the extent of disease: (*a*) one first treated by surgery, mainly with a solitary tumor or few tumors; and (*b*) the second treated with transcatheter arterial chemoembolization, mostly with multiple and advanced tumors. The serum level of sGPC3 was 2.61 ± 2.69 ng/ml for the former group,

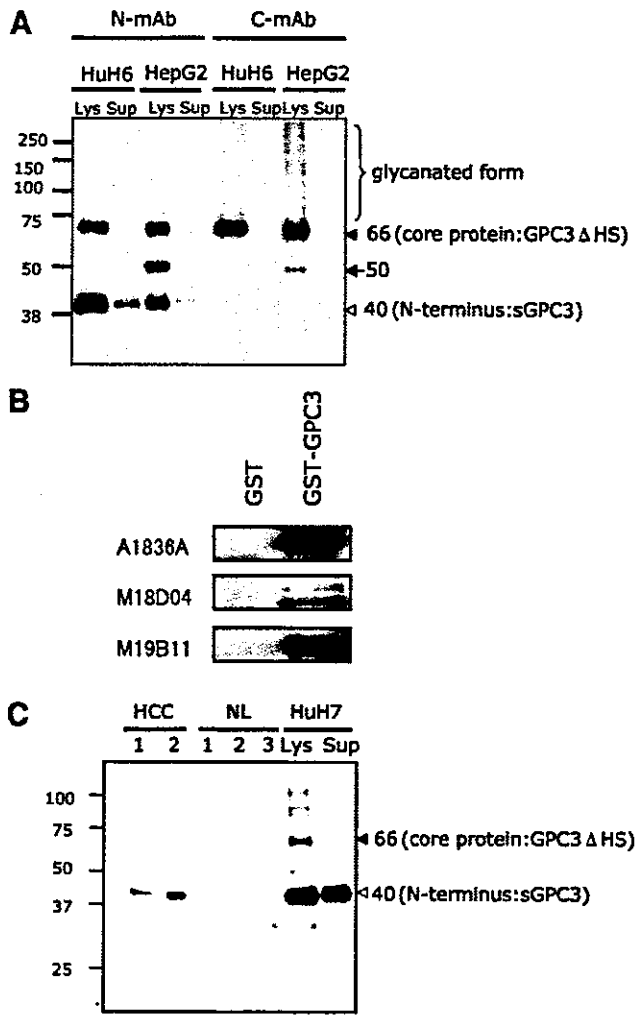

Fig. 2. Characterization of endogenous glypican-3 (GPC3) proteins with monoclonal antibodies (mAbs). *A*, representative immunoblotting of endogenous GPC3 in the cell lysate and culture supernatant with N-mAb and C-mAb. HepG2 and HuH6 were analyzed. Note that soluble GPC3 (sGPC3) alone is detected in the culture supernatant. *Brace*, glycanated GPC3 (smearing); *closed arrowhead*, core protein of GPC3 (M_r 66,000); *open arrowhead*, sGPC3 (M_r 40,000); *arrow*, uncharacterized processed fragment of GPC3 (M_r 50,000). *Lys*, lysate; *Sup*, supernatant of culture media. *B*, immunoblotting analysis with anti-GPC3 antibodies A1836A, M18D04, and M19B11 recognized glutathione *S*-transferase-sGPC3 but did not recognize glutathione *S*-transferase. *C*, detection of sGPC3 alone in the sera of the patients with hepatocellular carcinoma. Sera from two patients with hepatocellular carcinoma and three healthy adults (NL) were analyzed by immunoprecipitation with M18D04 followed by immunoblotting with A1836A. HuH7 cells were analyzed as a reference. *Closed arrowhead*, core protein of GPC3 (M_r 66,000); *open arrowhead*, sGPC3 (M_r 40,000).

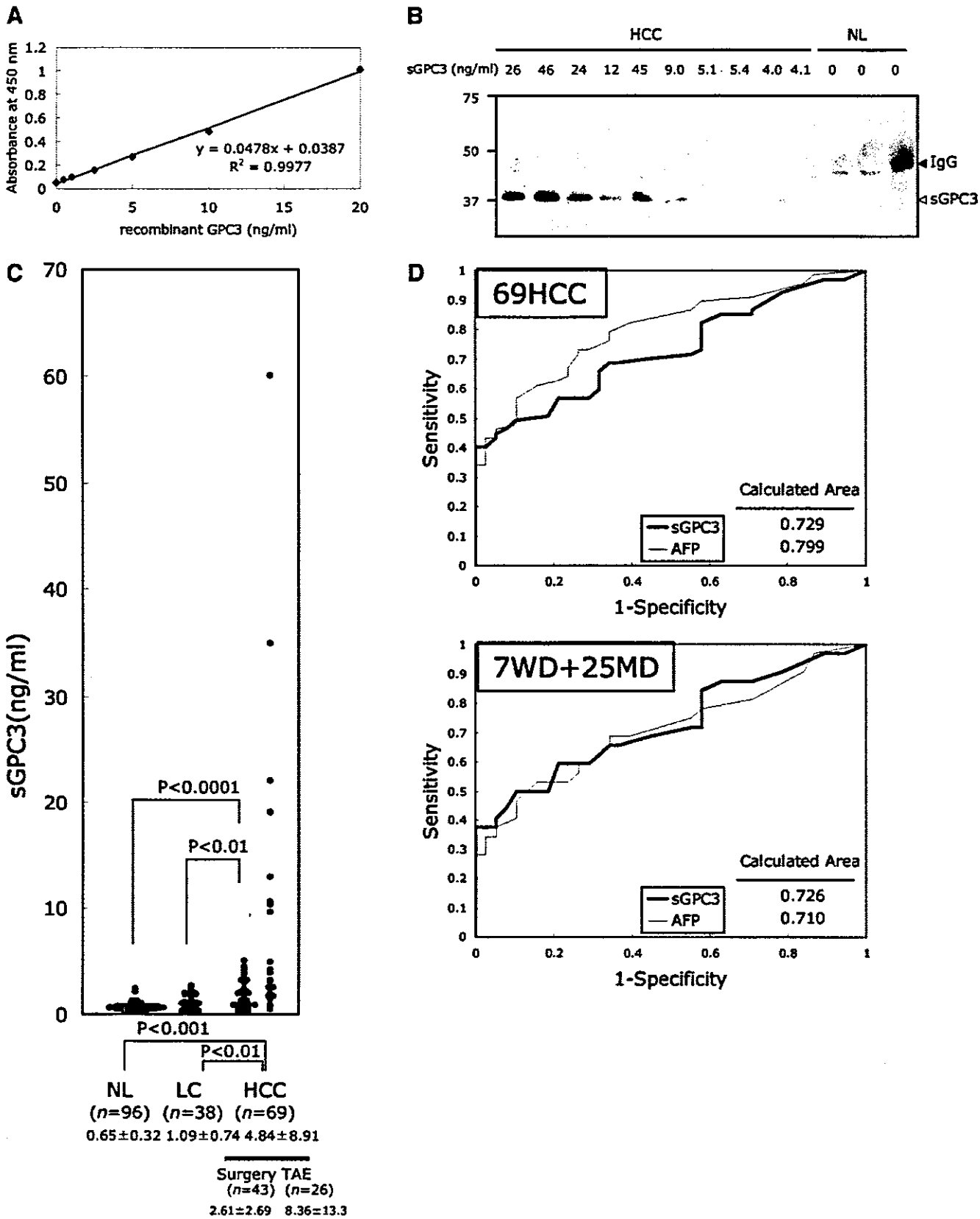

Fig. 3. Evaluation of soluble glypican-3 (sGPC3) as a serological marker of hepatocellular carcinoma (HCC). *A*, standard curve of sandwich ELISA. *B*, high specificity of sandwich ELISA. Specific detection of sGPC3 alone solely in the sera with elevated sGPC3 level measured with sandwich ELISA. Sera from 10 patients with HCC and 3 healthy adults (*NL*) were analyzed by immunoprecipitation with M18D04 followed by immunoblotting with A1836A. Serum sGPC3 level is indicated for each sample. *Open arrowhead*, sGPC3 (M_r 40,000); *closed arrowhead*, IgG. *C*, distribution of sGPC3 in the sera of patients with normal liver, liver cirrhosis (*LC*), and HCC (surgery and transcatheter arterial chemoembolization subgroup). Mean ± SD (ng/ml) of serum sGPC3 is indicated. Number of samples is indicated as *n*. *D*, receiver-operating characteristic curve analysis of sGPC3 (*thick line*) and α-fetoprotein (*thin line*). *Top panel*, all of the 69 HCCs and 38 cases of LC were included in the analysis. *Bottom panel*, 32 HCCs (including 7 well-differentiated and 25 moderately differentiated HCCs) and 38 cases of LC were analyzed. Area under the receiver-operating characteristic curve is indicated.

significantly higher than that for NL ($P < 0.0001$, Student's t test) or LC ($P < 0.01$), and 8.36 ± 13.3 ng/ml for the latter group (Fig. 3*C*), suggesting that the serum level of sGPC3 is elevated in an earlier stage and rises as HCC progresses. We then evaluated sGPC3 as a marker for HCC in relatively early-stage disease. When 43 cases treated by surgery were confined to 32 cases with relatively early-stage HCC (7 cases with WD HCC and 25 cases with MD HCC), calculated areas under the receiver-operating characteristic curve for sGPC3 and AFP were 0.726 and 0.710, respectively, indicating that sGPC3 is superior to AFP (Fig. 3*D*). The sensitivity of sGPC3 and AFP for the diagnosis of WD HCC and MD HCC was 50% and 47%, respectively. Moreover, combination measurement of both markers in WD HCC and MD HCC also markedly improved sensitivity to 72%. These results clearly demonstrate the utility of sGPC3 as a serological marker for HCC, especially for relatively early-stage HCC, and its complementarity to AFP.

DISCUSSION

GPC3 (alternatively called OCI-5 or MXR-7) is a heparan sulfate proteoglycan. The structural characteristics of the glypican family are (*a*) a core protein of approximately M_r 60,000, (*b*) binding to the membrane through GPI anchor, (*c*) heparan sulfate glycosaminoglycan attachment at Ser-Gly sequence within the COOH-terminal portion, and (*d*) a highly conserved pattern of 14 Cys residues (19). *GPC3* was originally isolated as a gene that is developmentally expressed in fetal rat intestine (21, 22). Mutation of *GPC3* is found in Simpson-Golabi-Behmel syndrome characterized by an overgrowth phenotype, hence its putative function was associated with an apoptotic effect (23). Silencing of *GPC3* in some types of cancer (24–26) is in line with this notion.

Overexpression of *GPC3* mRNA in HCC has been reported by ourselves and several other groups (15–18), although the role of GPC3 in carcinogenesis or progression of HCC has yet to be determined. In general, transcription level and protein level do not necessarily correlate. We have succeeded previously in generating an anti-GPC3 mAb against a peptide within the COOH-terminal portion, and we demonstrated using the antibody that the expression level of GPC3 core protein correlated well with its transcription level and that GPC3 was also overexpressed at protein level for the first time (15). Difficulties in making high-affinity antibodies against GPC3 (27), presumably due to its complex structure derived from disulfide bonds between 14 Cys residues, prohibited further analysis. We tried to generate high-affinity mAbs again by using recombinant GPC3 protein expressed in mammalian cells as an immunogen, and we finally succeeded in generating numerous high-affinity mAbs; to our knowledge, this is the first establishment of mAbs that can react with sGPC3. We did not recognize sGPC3 in a previous study (15) because we used a mAb against a relatively COOH-terminal portion (amino acids 355–371).

In the present work, we have precisely characterized GPC3 and demonstrated that the M_r 40,000 protein, sGPC3, derives from the NH_2-terminal portion of GPC3 and is cleaved between Arg^{358} and Ser^{359}. The M_r 40,000 protein was previously described by Mast *et al.* (19), who were searching for the binding protein on the plasma membrane of HepG2 cells for tissue factor pathway inhibitor. They purified a M_r 40,000 protein from culture supernatant of HepG2 cells and showed that it was derived from the NH_2-terminal portion of GPC3. They did not identify a cleavage site for the protein, unlike our study, but it is highly likely that the soluble protein they observed is sGPC3. They described purification of a M_r 40,000 protein only when protease inhibitors were used throughout the procedure, strongly suggesting that GPC3 cleavage is mediated by a protease (19). In addition, they found that washing the cells with dextran sulfate or heparin released significantly higher amounts of GPC3 than seen before treatment, strongly suggesting that most GPC3 is noncovalently attached to the cell surface after cleavage of the GPI anchor, but not in the culture supernatant (19). Our finding that sGPC3 alone is the major form of GPC3 in the culture supernatant of hepatoma cells and the serum of patients with HCC is consistent with these findings.

Very recently, two other groups reported elevated levels of GPC3 in the serum of HCC patients. The results still seem preliminary, although they are quite similar to ours. Here, we have made significant improvements in the reliability of the assay. Nakatsura *et al.* (28) used a polyclonal antibody raised against 303–464 amino acids of GPC3 in their analysis. The specificity of their ELISA is to be confirmed because it is not sandwich ELISA, despite the many nonspecific bands the antibody detected in their immunoblotting. Moreover, the standard used in the assay was not recombinant GPC3 but a supernatant of HepG2 cells that is a mixture of many heterogeneous proteins. It is possible that they are measuring a mixture of nonspecific but HCC-related proteins. Capurro *et al.* (29) used a polyclonal antibody and a mAb, both raised against the last 70 amino acids of the COOH-terminal portion of GPC3, to detect glycanated GPC3 in serum with their sandwich ELISA. However, the major detectable form of GPC3 in serum is sGPC3, which cannot be detected with these antibodies against the COOH-terminal portion, as shown clearly in the present study. In fact, we examined many combinations of mAbs in our sandwich ELISA, but we could detect signal only when we used a combination of two N-mAbs (data not shown). Furthermore, the only evidence reported previously for the extracellular localization of glycanated GPC3 is immunoblotting of HepG2 cell culture supernatant, rather than serum from HCC patients. Here, we demonstrated that sGPC3 is in the culture supernatant and serum of the HCC patients using both immunoblotting and sandwich ELISA with the same combination of mAbs. One possible interpretation of the result, obtained by Capurro *et al.*, is that they are detecting some short fragments derived from a COOH-terminal portion but not the glycanated form of GPC3, and this issue should be further investigated.

We have delineated the usefulness of sGPC3 as highly sensitive to early-stage HCC. In addition, there were several cases with elevated serum sGPC3 among LC patients, although not included in this study, where HCC developed within 6 months after serum examination or some tumor was already detected by ultrasound without final diagnosis of HCC by computed tomography or angiography. We have also demonstrated the complementarity of sGPC3 to another HCC marker, AFP. These findings promise future bedside use of sGPC3 as a serological marker of HCC. Another attractive aspect of GPC3 is that the membrane-anchored portion is a potential target for antibody therapy. In this context, diagnosis with serum sGPC3 is useful not only in early detection of HCC but also for future identification of patients with high sGPC3 levels for tailor-made HCC therapy. Thus, further investigation into the clinical aspects of GPC3 in HCC is warranted.

ACKNOWLEDGMENTS

We thank H. Meguro and S. Fukui for excellent technical assistance and H. Satoh for providing pGEX-5X-sGPC3 construct.

REFERENCES

1. Befeler AS, Di Bisceglie AM. Hepatocellular carcinoma: diagnosis and treatment. Gastroenterology 2002:122:1609–19.

2. Gebo KA, Chander G, Jenckes MW, et al. Screening tests for hepatocellular carcinoma in patients with chronic hepatitis C: a systematic review. Hepatology 2002;36: S84–92.
3. Johnson PJ. The role of serum α-fetoprotein estimation in the diagnosis and management of hepatocellular carcinoma. Clin Liver Dis 2001;5:145–59.
4. Taketa K. α-Fetoprotein: reevaluation in hepatology. Hepatology 1990;12:1420–32.
5. Kanetaka K, Sakamoto M, Yamamoto Y, et al. Overexpression of tetraspanin CO-029 in hepatocellular carcinoma. J Hepatol 2001;35:637–42.
6. Kondoh N, Shuda M, Tanaka K, et al. Enhanced expression of S8, L12, L23a, L27 and L30 ribosomal protein mRNAs in human hepatocellular carcinoma. Anticancer Res 2001;21:2429–33.
7. Scuric Z, Stain SC, Anderson WF, Hwang JJ. New member of aldose reductase family proteins overexpressed in human hepatocellular carcinoma. Hepatology 1998; 27:943–50.
8. Tanaka K, Kondoh N, Shuda M, et al. Enhanced expression of mRNAs of antisecretory factor-1, gp96, DAD1 and CDC34 in human hepatocellular carcinomas. Biochim Biophys Acta 2001;1536:1–12.
9. Shirota Y, Kaneko S, Honda M, Kawai HF, Kobayashi K. Identification of differentially expressed genes in hepatocellular carcinoma with cDNA microarrays. Hepatology 2001;33:832–40.
10. Okabe H, Satoh S, Kato T, et al. Genome-wide analysis of gene expression in human hepatocellular carcinomas using cDNA microarray: identification of genes involved in viral carcinogenesis and tumor progression. Cancer Res 2001;61:2129–37.
11. Smith MW, Yue ZN, Geiss GK, et al. Identification of novel tumor markers in hepatitis C virus-associated hepatocellular carcinoma. Cancer Res 2003;63:859–64.
12. Xu XR, Huang J, Xu ZG, et al. Insight into hepatocellular carcinogenesis at transcriptome level by comparing gene expression profiles of hepatocellular carcinoma with those of corresponding noncancerous liver. Proc Natl Acad Sci USA 2001;98: 15089–94.
13. Chen X, Cheung ST, So S, et al. Gene expression patterns in human liver cancers. Mol Biol Cell 2002;13:1929–39.
14. Chuma M, Sakamoto M, Yamazaki K, et al. Expression profiling in multistage hepatocarcinogenesis: identification of HSP70 as a molecular marker of early hepatocellular carcinoma. Hepatology 2003;37:198–207.
15. Midorikawa Y, Ishikawa S, Iwanari H, et al. Glypican-3, overexpressed in hepatocellular carcinoma, modulates FGF2 and BMP-7 signaling. Int J Cancer 2003;103: 455–65.
16. Hsu HC, Cheng W, Lai PL. Cloning and expression of a developmentally regulated transcript MXR7 in hepatocellular carcinoma: biological significance and temporospatial distribution. Cancer Res 1997;57:5179–84.
17. Zhu ZW, Friess H, Wang L, et al. Enhanced glypican-3 expression differentiates the majority of hepatocellular carcinomas from benign hepatic disorders. Gut 2001;48: 558–64.
18. Zhou XP, Wang HY, Yang GS, et al. Cloning and expression of MXR7 gene in human HCC tissue. World J Gastroenterol 2000;6:57–60.
19. Mast AE, Higuchi DA, Huang ZF, et al. Glypican-3 is a binding protein on the HepG2 cell surface for tissue factor pathway inhibitor. Biochem J 1997;327:577–83.
20. Niwa H, Yamamura K, Miyazaki J. Efficient selection for high-expression transfectants with a novel eukaryotic vector. Gene (Amst.) 1991;108:193–9.
21. Filmus J, Church JG, Buick RN. Isolation of a cDNA corresponding to a developmentally regulated transcript in rat intestine. Mol Cell Biol 1988;8:4243–9.
22. Filmus J. Glypicans in growth control and cancer. Glycobiology 2001;11:19R–23R.
23. Pilia G, Hughes-Benzie RM, MacKenzie A, et al. Mutations in GPC3, a glypican gene, cause the Simpson-Golabi-Behmel overgrowth syndrome. Nat Genet 1996;12: 241–7.
24. Lin H, Huber R, Schlessinger D, Morin PJ. Frequent silencing of the GPC3 gene in ovarian cancer cell lines. Cancer Res 1999;59:807–10.
25. Xiang YY, Ladeda V, Filmus J. Glypican-3 expression is silenced in human breast cancer. Oncogene 2001;20:7408–12.
26. Kim H, Xu GL, Borczuk AC, et al. The heparan sulfate proteoglycan GPC3 is a potential lung tumor suppressor. Am J Respir Cell Mol Biol 2003;6:694–701.
27. Filmus J, Shi W, Wong ZM, Wong MJ. Identification of a new membrane-bound heparan sulphate proteoglycan. Biochem J 1995;311:561–5.
28. Nakatsura T, Yoshitake Y, Senju S, et al. Glypican-3, overexpressed specifically in human hepatocellular carcinoma, is a novel tumor marker. Biochem Biophys Res Commun 2003;306:16–25.
29. Capurro M, Wanless IR, Sherman M, et al. Glypican-3: a novel serum and histochemical marker for hepatocellular carcinoma. Gastroenterology 2003;125:89–97.

Oncogene (2004) 23, 726–734

www.nature.com/onc

STAT3 and MITF cooperatively induce cellular transformation through upregulation of c-*fos* expression

Akiko Joo[1], Hiroyuki Aburatani[2], Eiichi Morii[3], Hideo Iba[4] and Akihiko Yoshimura*[,1]

[1]*Division of Molecular and Cellular Immunology, Medical Institute of Bioregulation, Kyushu University, 3-1-1 Maidashi, Higashi-ku, Fukuoka 812-8582, Japan;* [2]*Division of Genome Science, Research Center for Advanced Science and Technology, The University of Tokyo, Komaba, Meguro-ku, Tokyo 153-8904, Japan;* [3]*Department of Pathology, Osaka University Medical School, 2-2 Yamadaoka, Suita, Osaka 565-0871, Japan;* [4]*Institute of Medical Science, The University of Tokyo, Shirokane-dai, Minato-ku, Tokyo 108-8639, Japan*

The signal transducer and activator of transcription (STAT) family proteins are transcription factors critical in mediating cytokine signaling. Among them, STAT3 is frequently activated in a number of human cancers and transformed cell lines and is implicated in tumorigenesis. However, although constitutively activated STAT3 mutant (STAT3C) leads to cellular transformation, its transformation potential such as colony-forming activity in soft-agar is much weaker than that of v-src. To identify tumorigenic factors that cooperatively induce cellular transformation with STAT3C, we screened the retroviral cDNA library. We found that the microphthalmia-associated transcription factor (MITF), an essential transcription factor for melanocyte development and pigmentation, induces anchorage-independent growth of NIH-3T3 cells in cooperation with STAT3C. Microarray analysis revealed that c-*fos* is highly expressed in transformants expressing STAT3C and MITF. Promoter analysis and chromatin immunoprecipitation assay suggested that both STAT3 and MITF can cooperatively upregulate the c-*fos* gene. In addition, the transformation of NIH-3T3 cells by both MITF and STAT3C was significantly suppressed by a dominant-negative AP-1 retrovirus. These data indicate that MITF and STAT3 cooperatively induce c-*fos*, resulting in cellular transformation.
Oncogene (2004) **23**, 726–734. doi:10.1038/sj.onc.1207174

Keywords: MITF; STAT3; c-*fos*; cellular transformation

Introduction

The signal transducer and activator of transcription (STAT) family proteins were identified in the last decade as transcription factors essential for mediating virtually all cytokine signaling (Darnell, 1997; Stark *et al.*, 1998). These proteins become activated through tyrosine phosphorylation. In addition to their central roles in normal cell signaling, recent studies have demonstrated that constitutively activated STAT signaling, especially STAT3, directly contributes to oncogenesis (Bromberg and Darnell, 2000). For example, all *src*-transformed cell lines exhibit constitutively activated STAT3 (Yu *et al.*, 1995), and dominant-negative STAT3 suppresses *src* transformation without having any effect on *ras* transformation (Turkson *et al.*, 1998). More directly, Bromberg *et al.* (1999) demonstrated that a constitutively activated form of STAT3, STAT3C, which has two substituted cysteine residues within the C-terminal loop of the SH2 domain, resulting in a spontaneous transcriptionally active dimer, causes cellular transformation scored by colony formation in soft-agar and tumor formation in nude mice. Thus, the activated STAT3 molecule by itself can mediate cellular transformation. Extensive surveys of primary tumors and cell lines derived from tumors have indicated that an inappropriate activation of STAT3 occurs at a surprisingly high frequency in a wide variety of human cancers (Bowman *et al.*, 2000). However, until now, mutations in the STAT3 gene have not been identified in these cancers, hence it remained to be determined how endogenous STAT3 is constitutively activated and what kinds of genes are involved in tumorigenicity induced by constitutively activated STAT3.

The microphthalmia-associated transcription factor (MITF) is a basic helix–loop–helix leucine zipper (b-HLH-Zip) transcription factor that plays a critical role in the differentiation of various cell types, including neural crest-derived melanocytes, mast cells, osteoclasts, and optic cup-derived retinal pigment epithelium. MITF mutations in humans produce auditory–pigmentary syndromes, such as Waardenburg syndrome type IIa and Tietz syndrome, characterized by mast cell defects, inner ear problems, and abnormal, patchy pigmentation of the hair and skin. In mice, the *mi* allele protein with the deletion of 216R in the basic region is known as a dominant-negative form through the sequestration of wild-type partners in non-DNA-binding dimmers. In addition to the complete absence of melanocytes, MITF dominant-negative mutants exhibit osteopetrosis (Kitamura *et al.*, 2002). MITF consists of at least five

*Correspondence: A Yoshimura; E-mail: yakihiko@bioreg.kyushu-u.ac.jp
Received 24 June 2003; revised 4 September 2003; accepted 5 September 2003